CD146^{+} Nanovesicles from Human Tonsil-Derived Mesenchymal Stem Cells Reduce Cellular Senescence and Reverse Aging in Skin, Brain, and Liver of Mouse Model.

Hong Bae Jeon

The Graduate School
Yonsei University
Department of Medicine

CD146^{+} Nanovesicles from Human Tonsil-Derived Mesenchymal Stem Cells Reduce Cellular Senescence and Reverse Aging in Skin, Brain, and Liver of Mouse Model.

A Dissertation Thesis Submitted
to the Department of Medicine
and the Graduate School of Yonsei University
in partial fulfillment of the
requirements for the degree of
Doctor of Philosophy in Medical Science

Hong Bae Jeon

December 2024

This certifies that the Dissertation of Hong Bae Jeon is approved

Thesis Supervisor	Won Jai Lee
Thesis Committee Member	Dong Won Lee
Thesis Committee Member	Tai Suk Roh
Thesis Committee Member	Dong Hee Kang
Thesis Committee Member	Ju Hee Lee

The Graduate School
Yonsei University
December 2024

TABLE OF CONTENTS

LIST OF FIGURES

ABSTRACT

CD146$^+$ Nanovesicles from Human Tonsil-Derived Mesenchymal Stem Cells Reduce Cellular Senescence and Reverse Aging in Skin, Brain, and Liver of Mouse Model.

Cellular senescence, a defining aspect of aging, greatly contributes to the progressive dysfunction of tissues and organs that accompany the aging process. Recently, nanovesicles (NV), which are derived from tonsil mesenchymal stem cells (MSCs) (TMSC-NVs), have been investigated for their potential to reverse cellular senescence, particularly oxidative stress-induced senescence. However, the mechanisms by which TMSC-NVs control this process remain unclear. In this study, we focused on CD146, a surface marker utilized to determine specific MSC subgroups, and examined the therapeutic roles and antiaging potential of CD146$^+$ TMSC-NVs. We used a passage-associated senescence model of human dermal fibroblasts (HDFs), which is an *ex vivo* model of human skin photoaging caused by ultraviolet B (UVB) radiation, and a natural aging mouse model.

Our results indicate that CD146$^+$ TMSC-NVs treatment significantly promoted cell proliferation and increased collagen type I (COL1), Elastin, and antioxidant gene expressions by 530%, 665%, and 971%, respectively, compared with old HDFs. Microarray analysis revealed differential expressions of senescence-related genes in CD146$^+$ TMSC-NVs-treated HDFs compared with untreated old HDFs, with the gene expression profile of treated cells closely resembling that of young HDFs. Gene ontology and Kyoto Encyclopedia of Genes and Genomes enrichment analyses were conducted to investigate the therapeutic mechanisms underlying the antiaging effects. The results indicated that CD146$^+$ TMSC-NVs downregulated the cellular senescence pathway at the gene level, highlighting their potential antiaging effects.

CD146$^+$ TMSC-NVs (50 and 100 μg/ml) were applied to the *ex vivo* model of human skin photoaging induced by UVB radiation according to the results of the passage-associated senescence model of HDFs. The results revealed a significant increase in COL1, COL3, and Elastin expressions by 91%, 87%, and 10%, respectively, in the dermis of the group treated with CD146$^+$ TMSC-NVs of 50 μg/ml compared with the UVB group. However, the expression of matrix metalloproteinase 13 (MMP-13) decreased by 45% compared with that of the UVB group. Significant increases in involucrin, filaggrin, and loricrin expressions by 250%, 340%, and 114%, respectively, were observed in the epidermis in the group treated with CD146$^+$ TMSC-NVs of 50 μg/ml compared with the UVB group. These results indicated that CD146$^+$ TMSC-NVs improved the extracellular matrix (ECM) in the dermis and improved the skin barrier function through increased epidermal production, emphasizing their potential for skin rejuvenation applications.

The relative COL1 expression decreased significantly by 8% in the old skin compared to the young skin in the natural aging mouse model, whereas Elastin expression was increased by 10%. CD146$^+$ TMSC-NVs increased COL1 expression by 14% compared to the old group and decreased Elastin expression by 5%. Immunohistochemical analysis revealed that the CD146$^+$ TMSC-NVs

treatment group demonstrated a significant reduction in p-Tau expression in the brain by 47% compared with the old group, resembling the levels observed in the young group. Furthermore, $CD146^+$ TMSC-NVs treatment reduced Aβ expression by 41%. Western blot analysis revealed that the $CD146^+$ TMSC-NVs treatment group demonstrated a reduction in p-Tau and Aβ expression compared with the old group, whereas $CD146^-$ TMSC-NVs exhibited no comparable effect. All treatment groups, including the TMSC-NVs, $CD146^+$ TMSC-NVs, and $CD146^-$ TMSC-NVs, demonstrated reductions in α-SMA expressions in the liver by 16%, 24%, and 38%, respectively, compared with the old group. However, no significant differences in perilipin-1 expression were observed between the old and all TMSC-NVs-treated groups.

In conclusion, $CD146^+$ TMSC-NVs effectively reduced cellular senescence and reversed aging in the skin, brain, and liver of mouse models. These results indicate the significant therapeutic potential of $CD146^+$ TMSC-NVs in antiaging treatments.

Key words: mesenchymal stem cells; cell-derived microparticles; cell senescence

I. INTRODUCTION

The global aging population is expected to reach unprecedented levels due to decreasing fertility rates and increasing life expectancy. This demographic change is related to an increased prevalence of age-related diseases, imposing a substantial burden on society, healthcare systems, and the economy. Half of the global population growth is expected to stem from an increase in individuals aged ≥60 years from 2010 to 2050. Furthermore, the population of those ≥60 years of age is expected to double, whereas the number of individuals <60 years of age is likely to decrease.[1,2] Aging is predominantly characterized by cognitive decline, cardiovascular impairments, tissue degeneration, and metabolic changes, which influence individuals at varying rates. Additionally, immune system senescence significantly contributes to age-related diseases, which are the leading causes of death after 65 years of age. Such diseases include arthritis, cardiovascular disease, cancer, dementia, osteoporosis, diabetes, hypertension, neuropathy, stroke, obesity, and depression.[3,4]

Aging is defined by the following nine key hallmarks: cellular senescence, mitochondrial dysfunction, epigenetic changes, deregulated nutrient sensing, genomic instability, altered intercellular communication, telomere shortening, and stem cell exhaustion.[5] It can be interpreted in terms of stem cells, which may play a pivotal role in regulating and affecting the progression of aging. Maintaining a delicate and dynamic balance within the stem cell niche is important for supporting their differentiation into diverse progenitor cells or lineages, potentially slowing down the aging process.[6]

However, research has increasingly focused on the regenerative potential of exosomes, which are nanosized biomimetic vesicles, considering that the limitations in the clinical application of stem cells become more apparent. Stem cell-derived exosomes are popular for their capacity to modulate the immune system, stimulate cell proliferation, increase angiogenesis, inhibit apoptosis, decrease oxidative stress, and prevent functional decline.[3,7] Exosomes have been extensively investigated for their potential in skin rejuvenation and antiaging therapies. Previous studies have revealed that exosomes derived from umbilical cord mesenchymal stem cells (MSCs) are absorbed by the human skin, thereby improving the synthesis of collagen I and Elastin, which are two key components of skin rejuvenation. These results indicate promising cosmetic and therapeutic applications for exosome-based treatments.[8]

Exosomes provide considerable therapeutic potential, but they present several difficulties, including low efficiency, prolonged procedures, and the need for specialized technical expertise. Additionally, ensuring size uniformity, content consistency, and high yield during the labor-intensive and time-consuming production processes remains a significant challenge.[9] To overcome these hurdles, exosome-mimetic NVs, which demonstrate similar characteristics to exosomes, have been used in tissue regeneration, wound healing, and antiaging therapies for the skin. Dohyun Kim et al. revealed that NVs derived from tonsil mesenchymal stem cells (TMSC-NVs) mitigated cellular senescence caused by oxidative stress.[10] However, the mechanism by which TMSC-NVs

control cellular senescence remains unclear.

CD146, also known as the melanoma cell adhesion molecule, is an antigen that is expressed on various epithelial cells, activated T cells, and dendritic cells.[11] It appeared as a valuable surface marker for determining specific MSC subpopulations. The $CD146^+$ MSC subgroup is known to demonstrate improved biological activity and greater therapeutic potential in regenerative medicine.[12] Previous studies have revealed that $CD146^+$ MSCs have strong immunomodulatory properties.[13] Furthermore, Lin Zhang et al. demonstrated that $CD146^+$ umbilical cord MSCs possess superior regenerative capabilities compared to $CD146^-$ MSCs in the context of premature ovarian failure.[14] However, the therapeutic potential of $CD146^+$ nanovesicles (NVs) derived from human tonsil-derived MSCs (TMSC-NVs) remains unknown.

Herein, we investigated the therapeutic roles of $CD146^{+/-}$ TMSC-NVs on cell proliferation and cellular senescence utilizing an *in vitro* study of a passage-associated senescence model of human dermal fibroblasts (HDFs). Microarray gene analysis was subsequently conducted to investigate the mechanisms underlying the antiaging effects. Additionally, an *ex vivo* model of human skin photoaging induced by ultraviolet B (UVB) radiation was utilized to assess the therapeutic potential of $CD146^{+/-}$ TMSC-NVs. Furthermore, histological skin, brain, and liver analyses were conducted following the intraperitoneal (IP) administration of $CD146^{+/-}$ TMSC-NVs in a natural aging mouse model.

II. Materials and Methods

2.1. Production of CD146 NVs derived from TMSCs

2.1.1. Identification of TMSCs

TMSCs were isolated from human tonsil tissue at the Department of Plastic and Reconstructive Surgery, Yonsei University College of Medicine, after each participant provided informed consent, as previously described.[10] Initially, the human tonsil tissue was rinsed with phosphate-buffered saline (PBS) (Welgene, Seoul, South Korea) supplemented with 2% antibiotics–antimycotics (Thermo Fisher Scientific, Waltham, MA, USA). Next, the tissue was finely minced and enzymatically digested using collagenase type 1 (Gibco, New York, NY, USA) of 210 U/mL and DNase 1 (Sigma, St. Louis, MO, USA) of 4 KU/mL in low-glucose Dulbecco's modified Eagle's medium (DMEM) (Gibco, New York, NY, USA) at 37°C for 90 min. The mixture was passed through a 40-μm strainer and centrifuged at 1,300 rpm for 3 min after digestion. The resultant cell pellet was washed with DMEM twice. Subsequently, the cells were cultured in DMEM supplemented with 10% fetal bovine serum (Gibco, New York, NY, USA) and 1% antibiotics–antimycotics under conditions of 37°C and 5% CO_2. The culture media were replaced every two days.

.

2.1.2. Isolation of $CD146^+$ TMSCs and $CD146^-$ TMSCs

TMSCs were separated into CD146-positive ($CD146^+$) and CD146-negative ($CD146^–$) cells at passages 2–4 using magnetic-activated cell sorting (MACS) following the manufacturer's instructions.[12] The cells were washed with PBS and trypsinized with TrypLE Express solution (Gibco, New York, NY, USA) at 37°C for 3 min. The suspended cells were washed with 0.5% BSA and ethylenediaminetetraacetic acid (EDTA) of 2 mM in PBS and then centrifuged at 1,300 RPM for 3 min. Cell pellets were incubated with FcR Blocking Reagent and CD146 MicroBeads (CD146 MicroBead Kit; Miltenyi Biotec Inc, Bergisch Gladbach, Germany) at 4°C for 20 min. $CD146^+$ and $CD146^–$ cells were distributed utilizing LS columns (130-042-401, Miltenyi Biotec Inc, Bergisch Gladbach, Germany). Both $CD146^+$ and $CD146^–$ cells were subsequently used in the experiments to manufacture the NVs.

2.1.3. Production of $CD146^{+/-}$ TMSC-NVs

Nanovesicles derived from TMSCs (TMSC-NVs), $CD146^+$ TMSCs ($CD146^+$ TMSC-NVs) and $CD146^–$ TMSCs ($CD146^-$ TMSC-NVs) were manufactured as previous described.[10] The cells were washed with PBS and resuspended in PBS at a concentration of 1×10^6 cells/mL after separation. They were serially extruded through 10, 5, and 0.4 μm filters using a mini extruder (Avanti Polar Lipids, Alabaster, AL, USA) to manufacture the NVs. The ExoView R100 platform was used to analyze the CD9/CD63/CD81 phenotype and the size distribution of each NVs. The morphology of the NVs was analyzed with transmission electron microscopy (TEM). The protein concentration of the NVs was quantified with the Micro BCA™ Protein Assay Kit (Thermo Fisher Scientific, Waltham, MA, USA).

2.2. *In vitro* study of the passage-associated senescence model of HDFs

2.2.1. Cell culture

HDFs were obtained from the American Type Culture Collection (ATCC, Manassas, VA, USA). These cells were maintained in DMEM supplemented with 10% fetal bovine serum and 1% antibiotics–antimycotics at 37°C in a 5% CO_2 environment, with media changes every 2 days. Cellular senescence was induced through repeated cell passaging, with passage 3 cells classified as "young" and passage 15 cells as "old." The population of cells was assessed with the Cell Counting Kit 8 (CCK8) following the manufacturer's instructions (Dojindo). The optical density was measured at a 450 nm wavelength.

.

2.2.2. Senescence-Associated β-Galactosidase Assay

The Senescence-associated β-Galactosidase Assay (SA-β-galactosidase assay) was conducted using a cellular senescence staining kit (CBA-230, Cell Biolabs, San Diego, CA, USA) as previously described.[10] Cells were fixed with 0.25% glutaraldehyde solution at room temperature for 5 min. The supernatant was discarded after fixation, and each well was gently washed with fresh PBS three times. X-gal staining working solution was then added, and the cells were incubated overnight at 37°C. The supernatant was discarded after the reaction, and the cells were gently washed twice with PBS. Quantitative analysis was conducted by documenting the colorization ratio of the senescent cells.

2.2.3. Quantitative Real-Time Polymerase Chain Reaction (qPCR)

Total RNA was extracted with TRIzol Reagent (Ambion, Waltham, MA, USA) to confirm the RNA expression of the cells. TRIzol Reagent of 500 μL was applied to the cells 6 days after treatment of each NVs at 50 μg/mL. The reagent was treated with chloroform (Sigma, St. Louis, MO, USA) of 100 μL and incubated on ice for 15 min. The samples were centrifuged at 13,000 rpm for 15 min after incubation, and a transparent supernatant was obtained. The supernatant was treated with the same volume of isopropanol (Sigma, St. Louis, MO, USA), incubated at room temperature for 15 min, and centrifuged at 1,300 rpm for 15 min for RNA precipitation. The total RNA concentration was measured with NanoDrop 2000 (Thermo Fisher Scientific, Waltham, MA, USA) and a total RNA of 1 μg was used for cDNA synthesis with the PrimeScript™ RT Reagent (RR037A, Takara Bio Inc., Shiga, Japan) following the described procedure. Power SYBR™ Green PCR Master Mix (Applied Biosystems, San Francisco, CA, USA) was used for qPCR, and the reaction was measured with the StepOnePlus real-time PCR system (Applied Biosystems, San Francisco, CA, USA).

2.2.4. Microarray analysis

The Affymetrix Whole Transcript Expression array process was conducted by Macrogen, Inc. (Seoul, Korea) following the manufacturer's protocol (GeneChip Whole Transcript PLUS reagent Kit). All samples (n = 10) were prepared and isolated in triplicate. The GeneChip WT (Whole Transcript) Amplification kit was used to synthesize cDNA for the microarray analysis. The sense cDNA was then fragmented and biotin-labeled with TdT (terminal deoxynucleotidyl transferase) with the GeneChip WT Terminal labeling kit. The labeled DNA target of approximately 5.5 μg was hybridized to the Affymetrix GeneChip Mouse Clariom S Array at 45°C for 16 h. The hybridized

arrays were washed and stained on a GeneChip Fluidics Station 450 and scanned on a GCS3000 Scanner (Affymetrix). The data were processed with the Affymetrix® GeneChip Command Console® Software (AGCC, Thermo). RNA purity and integrity were evaluated with the ND-2000 Spectrophotometer (NanoDrop, Wilmington, USA) and the Agilent 2100 Bioanalyzer (Agilent Technologies, Palo Alto, USA). Gene Ontology (GO) and Kyoto Encyclopedia of Genes and Genomes (KEGG) pathway enrichment analyses were conducted to determine differentially expressed genes (DEGs) at the biological functional level.[15] DEGs related to aging were selected with the DAVID database (Database for Annotation, Visualization, and Integrated Discovery.[16] A p-value of <0.05 was considered statistically significant difference[17]. The expression data of the selected genes were subjected to hierarchical clustering and expressed as a heat map.

2.3. *Ex vivo* study of human skin photoaging induced by UVB radiation

The Yonsei University Health System, Severance Hospital, Institutional Review Board (4-2023-0160) approved the *ex vivo* study in this paper. Human skin was obtained by surgical procedure. Tissues were gently washed with 2% antibiotics–antimycotics in PBS, and the hypodermis was surgically discarded. Semisolid media was manufactured by mixing in a 1:5 ratio of 2% agarose and culture media. Human skin was placed on the well after dispensing the semisolid media in the 6-well plate. Ultraviolet B (UVB) was treated three times for 3 days with $CD146^+$ TMSC-NVs of 50 and 100 μg/ml. Tissues were fixed with 4% paraformaldehyde after 6 days and embedded in paraffin for histological analysis.

2.4. *In vivo* study of natural aging mouse model

2.4.1. Preparation of natural aging mice and IP administration of TMSC-NVs

The Institutional Animal Care and Use Committee of Yonsei University (IACUC No. 2022-0096) approved the *in vivo* study in this paper. A total of nine female C57BL/6 mice, two 2-month-old mice, and seven 26-month-old mice were utilized to assess the effects of the NVs. All mice were specific pathogen-free and maintained under the same environmental conditions without any food intake differences. The mice were housed in an animal facility and were treated following the Guide for the Yonsei Laboratory Animal Research Center. IP TMSC-NVs were administered upon completing the NVs preparation. Old mice were randomly categorized into four groups following the injection material: control group (n = 2), TMSC-NVs (n = 2), $CD146^+$ TMSC-NVs (n = 2), and $CD146^-$ TMSC-NVs (n = 1). The experimental groups were administered $CD146^{+/-}$ TMSC-NVs of 150 μg twice, with a 7-day interval between injections. In contrast, old mice in the control group were administered only PBS of 300 μL. Young mice were included for interage comparisons from other groups. All mice were sacrificed after 2 weeks of treatment, and their skin, brain, and liver

were obtained for subsequent experimental analysis.

2.4.2. Histological analysis of skin, brain, and liver.

The skin, brain, and liver were obtained from the euthanized mice 2 weeks after completing the TMSC-NVs injection. These tissues were fixed in 4% formaldehyde for over 48 h at 4°C. They were cut into 4-μm slices following the paraffin embedding and stained with hematoxylin and eosin (H&E) and Masson's Trichrome (MT) for histological evaluation using standard procedures. Their morphology was observed with a light microscope (BX53, Olympus, Tokyo, Japan).

2.5. Immunohistochemistry analysis.

The samples were fixed in formaldehyde at 37°C before being embedded in paraffin wax. The paraffin-embedded tissues were sectioned into 4-μm-thick sections with a microtome. Heat-induced antigen retrieval was performed with sodium citrate buffer (S4641-500G, Sigma-Aldrich, St. Louis, USA) of 10 mM supplemented with 0.05% Tween 20 (69295S1601, Junsei, Tokyo, Japan) after deparaffinization using xylene and hydration with graded EtOH. Peroxidase was blocked with BLOXALL® Endogenous Blocking Solution (SP-6000-100, Vector Laboratories, Inc., CA, USA) at room temperature for 10 min after antigen retrieval. Afterward, 1.5% of normal horse serum (S-2000-20, Vector Laboratories, Inc., CA, USA) was treated for 30 min. Additionally, primary anticollagen type I (COL1), anticollagen type III (COL3), antimatrix metalloproteinase13 (MMP13), antiInvolucrin, antifibroblast, antiLoricrin, antiElastin, antiphosphor-Tau (p-Tau), antiamyloid beta (Aβ), antialpha-smooth muscle actin (α-SMA) and antiperilipin-1 antibodies were separately utilized overnight at 4 °C. All antibodies were used at a 1:200 dilution and purchased from Abcam. Biotinylated Goat antiRabbit IgG Antibody (H+L) (BP-9100-50, Vector Laboratories, Inc., CA, USA) and VECTASTAIN® Elite® ABC-HRP Reagent (PK-7100, Vector Laboratories, Inc., CA, USA) were used for 30 min each after washing with 0.05% Tween 20 in PBS. DAB staining was conducted using DAB Substrate Kit (SK-4100, Vector Laboratories, Inc., CA, USA) to detect the protein of interest, and Mayer's hematoxylin solution (AB220365, Abcam, Cambridge, UK) was utilized for nuclei counterstaining. The slides were photographed with an optical microscope (Olympus, IX73-F22PH, Tokyo, Japan). Slides can be analyzed in full or sampled using small boxes randomly scattered across the tissue area. The color deconvolution method was adopted using Fiji ImageJ open software to quantify the staining.[18]

2.6. Western blot analysis.

Protein extraction from brain tissues was performed as previously described.[19] Briefly, the tissues were homogenized in a lysis buffer containing TRIS of 500 mM, 2% SDS, EDTA of 25 mM, NaCl of 100 mM, 1% (v/v) triton X-100, and 1% (v/v) NP-40, supplemented with DTT (Merck, Rahway, NJ, USA) of 10 mM, as well as protease and phosphatase inhibitors (Thermo Fisher Scientific). The homogenates were incubated at 90°C for 2 h, followed by centrifugation at

12,000 g for 20 min at 4°C. The protein concentration was identified with the Pierce BCA Assay Kit (Thermo Fisher Scientific). Protein of 40 μg was separated by sodium dodecyl sulfate-polyacrylamide gel electrophoresis (SDS-PAGE) for each sample. Proteins were then transferred onto a nitrocellulose membrane (Bio-Rad, Hercules, CA, USA). The membranes were incubated overnight at 4°C with primary antibodies that target phosphor-Tau (p-Tau; Thermo Fisher Scientific) and amyloid beta (Aβ; Thermo Fisher Scientific). The membranes were incubated with horseradish peroxidase-conjugated secondary antibodies (Cell Signaling Technology, Danvers, MA, USA) at room temperature for 1 h after the primary antibody incubation. Protein bands were visualized with the Supersignal West Pico Plus chemiluminescent substrate (Thermo Fisher Scientific), and images were captured with an iBright imaging system (Thermo Fisher Scientific). The level of each protein was quantified by normalizing its signal against that of β-actin.

2.7.Statistical analysis

In the present study, all experiments were repeated at least three times. Additionally, all graphs were drawn with GraphPad Prism 8.0.2 software (GraphPad Software Inc., San Diego, CA, USA) and are presented as mean ± standard error of the mean. Significant differences were identified using one-way analysis of variance (* $p < 0.05$, ** $p < 0.01$, *** $p < 0.001$, **** $p < 0.0001$).

III. Results

3.1. Characterization of $CD146^{+/-}$ NVs Derived from TMSCs

TMSCs were isolated and cultured from human tonsil tissues after tonsillectomy. The morphology of the TMSCs demonstrated a fibroblast-like morphology (Figure 1a). Flow cytometry analysis indicated that TMSCs expressed common MSC markers, including CD90, CD105, and CD73 (Figure 1b), consistent with previous results.[10] Furthermore, the tetraspanin CD9, CD63, and CD81 were determined as general NVs markers. TMSC-NVs were characterized using the ExoView R100 platform, TEM, and DLS after their production. TMSC-NVs were captured with specific antibody-coated spots against tetraspanin CD63, CD81, and CD9. The total fluorescent particle counts of TMSC-NVs on the tetraspanin capture spots were higher than the mouse IgG isotype control, as presented by the ExoView R100 platform (Figure 1c, d). These results indicate that the isolated vesicles from TMSCs achieved the criteria for exosomes, supporting further investigations of their therapeutic potential. Additionally, they demonstrated a spherical shape, with mean diameters of 83 nm for TMSC-NVs, 76 nm for $CD146^{+}$ TMSC-NVs, and 80 nm for $CD146^{-}$ TMSC-NVs (Figure 1e, f). These results indicate that TMSC-NVs' characteristics closely resemble those of exosomes.

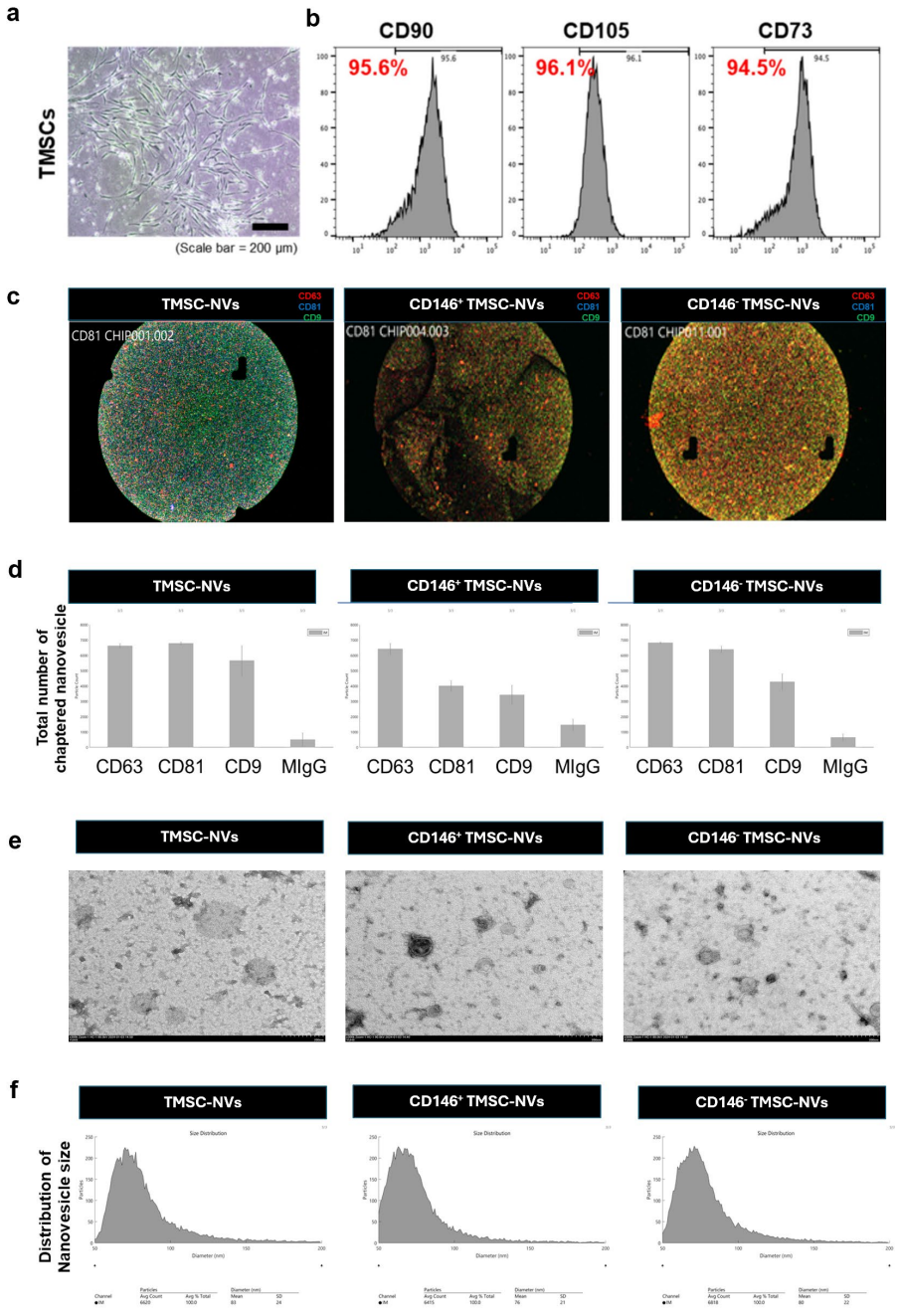

Figure 1. Characterization of CD146^{+} and CD146^{-} nanovesicles generated from tonsil-derived mesenchymal stem cells (TMSC- NVs). (a) Fibroblast-like morphology of TMSCs. (b) Flow

cytometry analysis revealing that TMSCs express common MSC markers, including CD90, CD105, and CD73. (c) ExoView R100 platform analysis demonstrating that TMSC-NVs were captured using specific antibody-coated spots against tetraspanin CD63, CD81, and CD9. (d) Total fluorescent particle counts of TMSC-NVs on tetraspanin capture spots were higher than the mouse IgG isotype control. (e) Spherical shape morphology of TMSC-NVs under a transmission electron microscope. (f) Size distribution and concentration analysis of the NVs showing mean diameters of 83 nm for TMSC-NVs, 76 nm for $CD146^+$ TMSC-NVs, and 80 nm for $CD146^-$ TMSC-NVs.

3.2. $CD146^+$ TMSC-NVs improved cell proliferation and increased ECM production and antioxidant gene in the passage-associated senescence model of HDFs

$CD146^{+/-}$ TMSC-NVs were applied to a passage-induced senescence model of HDFs, and the cell morphology was investigated. Figure 2a illustrates that the young HDFs demonstrated densely packed cultures with small, elongated cell bodies. In contrast, old HDFs exhibited morphological changes characterized by a larger, flattened shape and a near-transparent appearance in the treatment with $CD146^+$ TMSC-NVs. HDFs demonstrated increased density with smaller, elongated cell bodies. Subsequently, cell proliferation was evaluated using the CCK-8 assay. The results indicated that $CD146^+$ TMSC-NVs significantly promoted old HDF proliferation, indicating an 187% increase at 8 days, whereas $CD146^-$ TMSC-NVs exhibited no significant differences (Figure 2b).

The mRNA expression of the extracellular matrix (ECM) components and antioxidant genes associated with senescence was investigated with qPCR at the molecular level. After $CD146^{+/-}$ TMSC-NVs treatment, the expression levels of COL1, Elastin, and heme oxygenase 1 (HMOX1) were evaluated. The qPCR analysis revealed a significant upregulation in COL1 and Elastin expression in the $CD146^+$ TMSC-NVs group, with increases of 530% and 665%, respectively, compared with the reduced expression observed in old HDFs. Similarly, the expression of HMOX1, an antioxidant gene, was increased by 971% in old HDFs treated with $CD146^+$ TMSC-NVs compared with old HDFs (Figure 2c). These results indicate that $CD146^+$ TMSC-NVs stimulate HDF proliferation, improve ECM production, and increase antioxidant gene expression, thereby decreasing senescence in old cells.

.

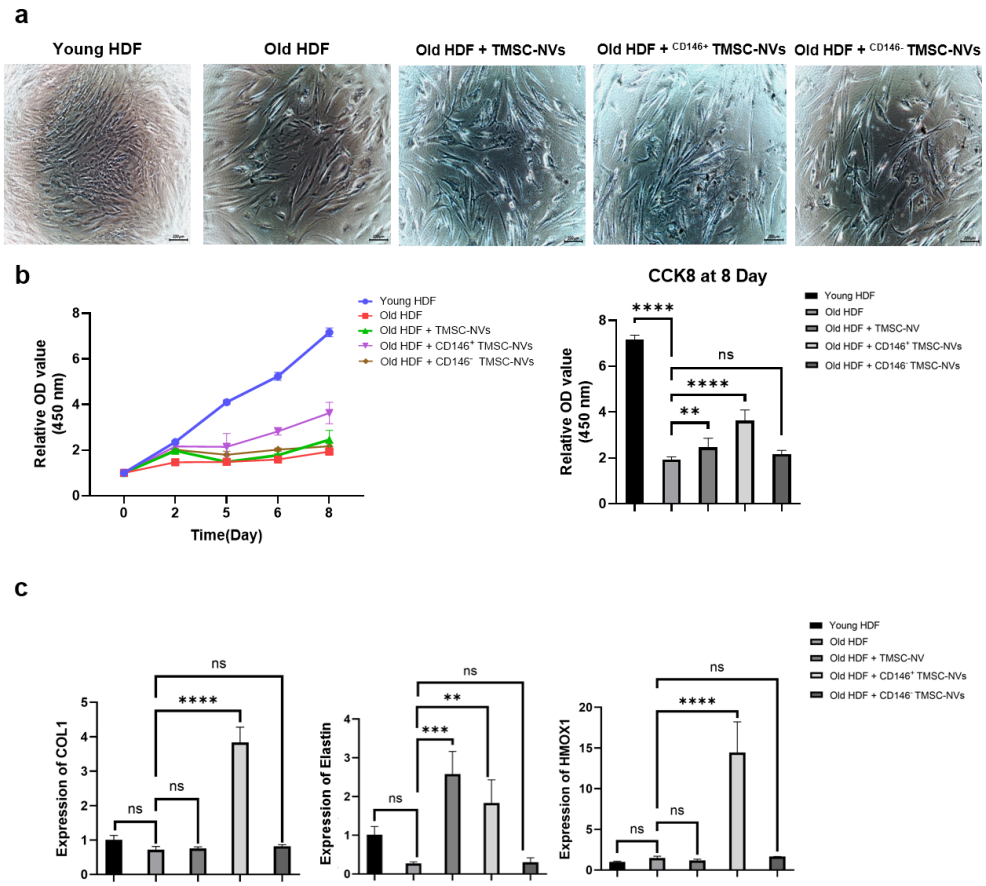

Figure 2. Regulation of cell proliferation, ECM, and antioxidant gene by TMSC- NVs treatment in the passage-associated senescence HDFs model. (a) Morphological changes in HDFs after TMSC-NVs treatment. (b) Cell proliferation test revealing that $CD146^+$ TMSC-NVs significantly promoted old HDF proliferation, showing a 187% increase at 8 days, whereas $CD146^-$ TMSC-NVs demonstrated no significant differences. (c) Reverse transcription-quantitative PCR exhibiting an increase in mRNA expression of COL1, Elastin, and heme oxygenase 1 (HMOX1), with 530%, 665%, and 971% increases, respectively, after $CD146^+$ TMSC-NVs treatment compared with untreated old HDFs. (* $p < 0.05$, ** $p < 0.01$, *** $p < 0.001$, **** $p < 0.0001$)

3.3. $CD146^+$ TMSC-NVs reduced cellular senescence in the passage-associated senescence model of HDFs, as demonstrated by the SA-β-galactosidase assay

The antiaging potential of TMSC-NVs was further assessed through the senescence-associated (SA) β-Galactosidase Assay. HDFs were subjected to the SA-β Gal staining, with Figure 3a illustrating the stained images. The percentage of blue-stained β-galactosidase-positive cells was lower in the young HDFs than in the old HDFs. Both $CD146^+$ TMSC-NVs and TMSC-NVs have reduced β-galactosidase activity in the old HDFs after treatment (Figure 3a).

Quantitative analysis from the SA-β-galactosidase assay subsequently revealed a 381% increase in the percentage of senescent cells in the old HDF than in the young HDF. In contrast, TMSC-NVs and $CD146^+$ TMSC-NVs treatment significantly reduced the percentage of senescent cells in the old HDF by 70% and 61%, respectively (Figure 3b). These results indicate that $CD146^+$ TMSC-NVs effectively reduce senescence caused by repeated passaging in HDFs.

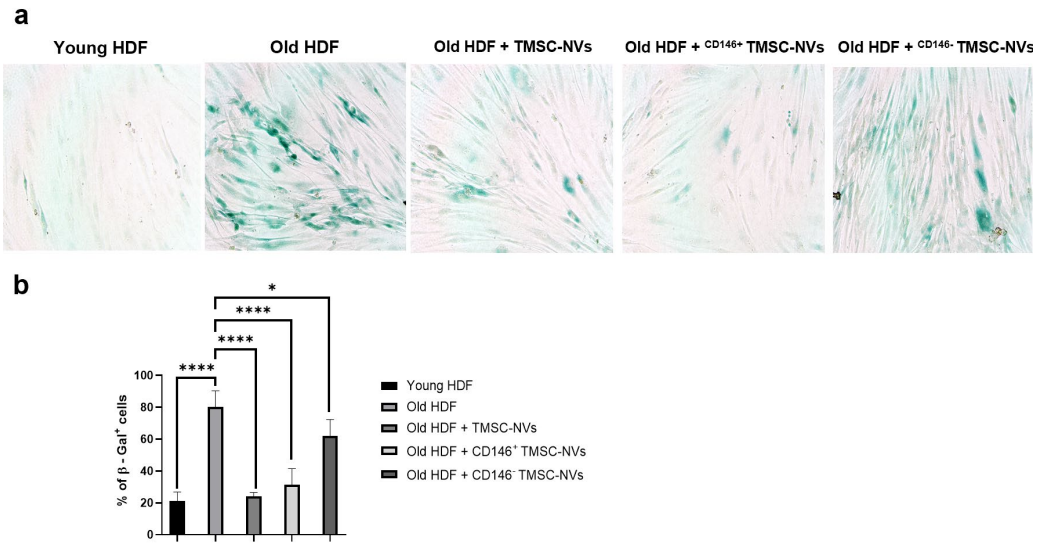

Figure 3. Regulation of senescence-associated (SA)-β-galactosidase activity by TMSC-NVs treatment in the passage-associated senescence HDFs model. (a) SA β-galactosidase assay revealing a lower percentage of blue-stained β-galactosidase-positive cells in the $CD146^+$ TMSC-NVs and TMSC-NVs treatment compared to old HDFs. (b) Quantitative analysis of SA-β-galactosidase activity indicating a 381% increase in the percentage of senescent cells in old HDF compared to Young HDF. TMSC-NVs and $CD146^+$ TMSC-NVs treatment significantly reduced the percentage of senescent cells in the old HDF by 70% and 61%, respectively. (* $p < 0.05$, ** $p < 0.01$, *** $p < 0.001$, **** $p < 0.0001$)

3.4. $CD146^+$ TMSC-NVs downregulate the cellular senescence pathway by microarray analysis in the passage-associated senescence model of HDFs

We conducted whole transcriptome analysis with the Affymetrix® WT Expression Microarray to comprehensively evaluate the effect of $CD146^+$ TMSC-NVs on the gene expression profile of HDFs. Genes with a fold change greater than the cut-off value (fold change >2 or < −2, $p < 0.05$) were classified as differentially expressed. A total of 3,226 out of 21,488 probes were determined as having different expressions among the HDF strain groups: young, old, TMSC-NVs, $CD146^+$ TMSC-NVs, and $CD146^-$ TMSC-NVs groups. These results are expressed as a heatmap (Figure 4a). The young group demonstrated 955 and 1,145 genes that were upregulated and downregulated, respectively, compared with the old group. The expression of 479 genes was increased in the $CD146^+$ TMSC-NVs group, whereas that of 411 was decreased as compared to the old group. The TMSC-NVs group exhibited 355 and 264 genes that were upregulated and downregulated, respectively. Similarly, 362 genes were upregulated, and 340 genes were downregulated in the $CD146^-$ TMSC-NVs group compared with the old group (Figure 4b). Subsequent analysis revealed that a significant proportion of these DEGs were related to aging, including senescence-related genes that were differentially expressed in HDFs treated with $CD146^+$ TMSC-NVs compared with old HDFs. The gene expression profile in the $CD146^+$ TMSC-NVs-treated HDFs closely resembled that of the young HDFs (Figure 4c).

GO and KEGG pathway enrichment analyses of DEGs were performed, comparing the old group with other groups, to investigate the potential antiaging mechanisms of $CD146^+$ TMSC-NVs. GO classification, according to biological processes, cellular components, and molecular functions, revealed that DEGs in the $CD146^+$ TMSC-NVs group were associated with processes similar to those observed in the young group when compared to the old group (Figure 4d). The KEGG pathway database includes pathway maps associated with metabolism, genetic information processing, environmental information processing, cellular processes, organismal systems, and human diseases. Supplementary Figure S1 illustrates a heat map illustrating the KEGG enrichment analysis. Figure 4e shows that the cellular senescence pathway was significantly downregulated in the young and $CD146^+$ TMSC-NVs group compared with the old group. In contrast, no significant differences were found in the $CD146^-$ TMSC-NVs and TMSC-NVs groups. DEGs in the cellular senescence pathway were mapped using color. Blue indicates downregulated genes, whereas red denotes upregulated genes in the $CD146^+$ TMSC-NVs groups compared with the old group. The downregulated genes consisted of CCND3, CCNE1, CCNE2, CDK2, and MYBL2, whereas the upregulated genes were RAD9A, GADD45A, EIF4EBP, and IL1A. These proteins are strongly related to cell cycle regulation, including processes such as cell cycle arrest and senescence-associated heterochromatin foci (SAHF) formation (Figure 4e). These results indicate that $CD146^+$ TMSC-NVs downregulate the cellular senescence pathway at the gene level, emphasizing their potential antiaging effects.

a

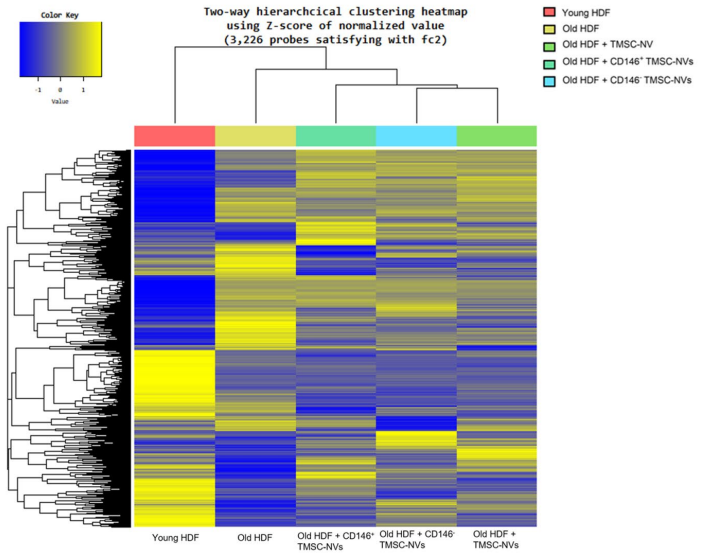

b

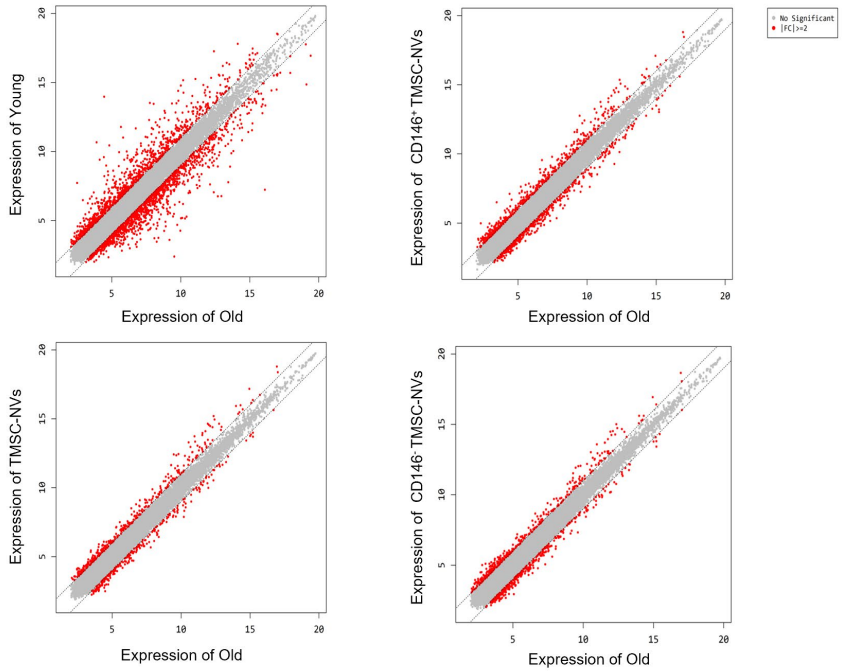

c

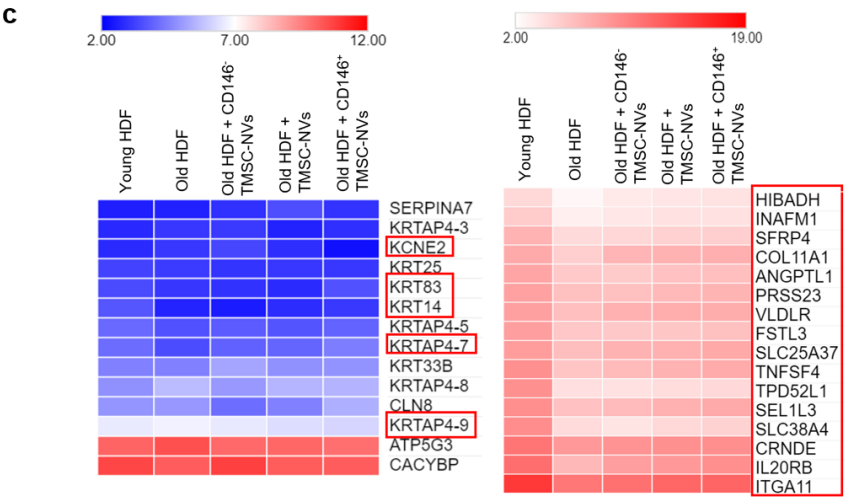

d

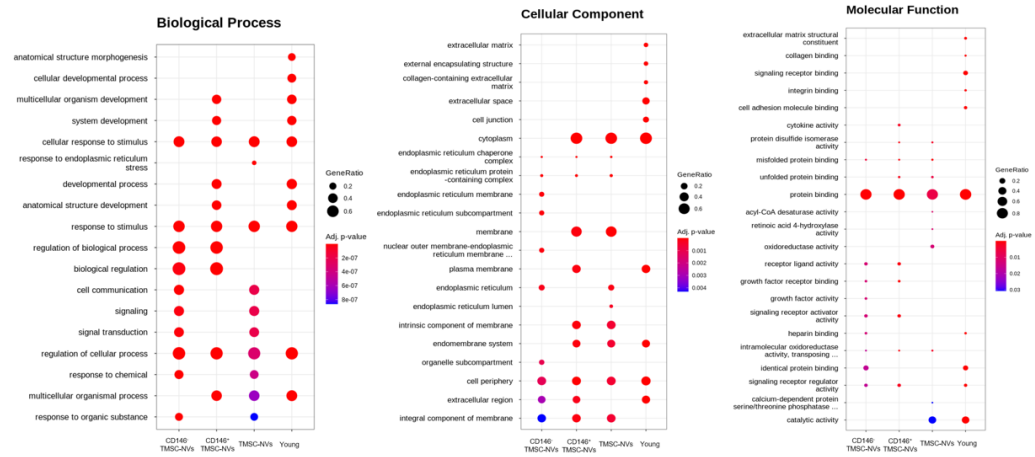

e

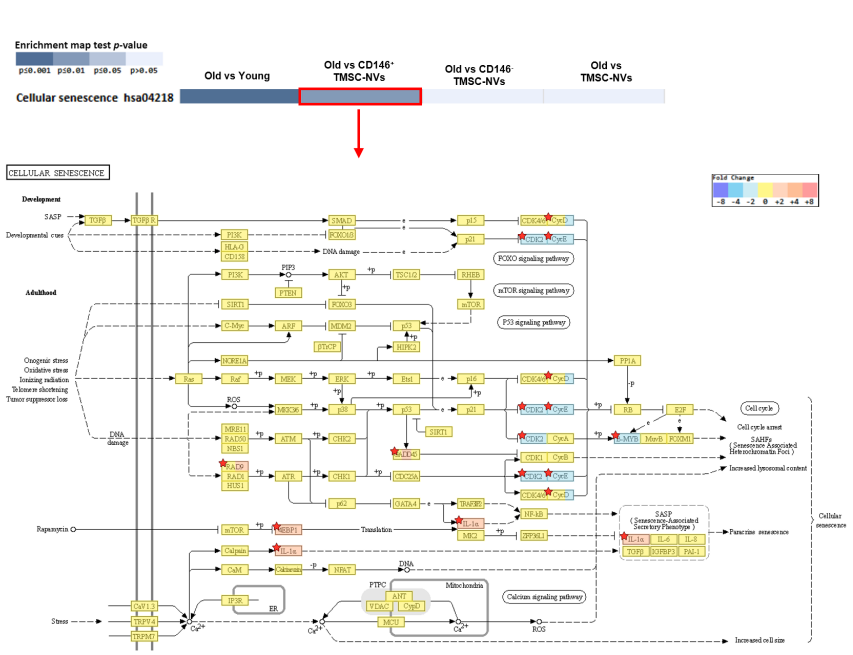

Figure 4. Regulation of the cellular senescence pathway by TMSC-NV treatment in the passage-associated senescence HDFs model. Affymetrix® WT Expression Microarray was utilized to assess the effect of TMSC-NVs on the gene expression profile of HDFs. (a) Genes with a fold change greater than the cutoff value (fold change >2 or < −2, $p < 0.05$) were classified as differentially expressed. A total of 3,226 out of 21,488 probes were determined as having different expressions among the HDF strain groups: young, old, TMSC-NVs, CD146$^+$ TMSC-NVs, and CD146$^-$ TMSC-NVs groups. (b) The young group exhibited 955 and 1,145 that were upregulated and downregulated, respectively, compared with the old group. Similarly, 479 genes were upregulated and 411 were downregulated in the CD146$^+$ TMSC-NVs group, whereas the TMSC-NVs group demonstrated 355 upregulated and 264 downregulated genes, and the CD146$^-$ TMSC-NVs group showed 362 upregulated and 340 downregulated genes compared with the old group. (c) A substantial proportion of these DEGs was related to aging. The gene expression profile, visualized as a heat map, demonstrated distinct expressions in CD146$^+$ TMSC-NV-treated HDFs, closely resembling those of young HDFs and differing from old HDFs. (d) GO classification revealed that DEGs in the CD146$^+$ TMSC-NV group were associated with processes similar to those observed in the young group when compared to the old group. (e) The cellular senescence pathway, among all KEGG pathways, exhibited significant differences in the young and CD146$^+$ TMSC-NVs groups compared to the old group. In contrast, no significant differences were found in the CD146$^-$ TMSC-NVs and TMSC-NVs groups. DEGs in the cellular senescence pathway were mapped using color. Blue indicates downregulated genes, while red indicates upregulated genes in the CD146$^+$ TMSC-NVs groups compared with the old group. The downregulated genes consisted of CCND3, CCNE1,

CCNE2, CDK2, and MYBL2, whereas the upregulated genes included RAD9A, GADD45A, EIF4EBP, and IL1A. These proteins are strongly associated with cell cycle regulation, including processes such as cell cycle arrest and senescence-associated heterochromatin Foci (SAHFs) formation.

3.5. An *ex vivo* study of human skin photoaging models revealed that CD146$^+$ TMSC-NVs increased the Col1 and Col2 and Elastin expression and decreased MMP-13 expression in the dermis.

CD146$^+$ TMSC-NVs were applied to the *ex vivo* model of human skin photoaging induced by UVB radiation according to the results of the passage-associated senescence model of HDFs. Cultured normal human skin samples were subjected to UVB irradiation, followed by treatment with varying CD146$^+$ TMSC-NV concentrations (50 and 100 μg/ml). Immunohistochemical (IHC) analyses with DAB staining were conducted to assess the expression of COL1, COL3, Elastin, and MMP-13 in the dermis.

Visual inspection revealed increased IHC DAB staining intensity for COL1, COL3, and MMP-13, with a decreased intensity for Elastin in the UVB group compared to the control group. CD146$^+$ TMSC-NV treatment at 50 μg/ml increased the staining for COL1, COL3, and Elastin compared with the UVB group while decreasing MMP13 staining (Figure 5a). These results were utilized for quantitative analysis to calculate the percentage of DAB-stained tissue, with DAB-stained regions marked on the original images. The results revealed a significant increase in COL1, COL3, and Elastin expressions by 91%, 87%, and 10%, respectively, in the group treated with CD146$^+$ TMSC-NV of 50 μg/ml compared with the UVB group. In contrast, MMP-13 expressions decreased by 45% relative to the UVB group. No significant differences in COL1 and COL3 levels were found between the CD146$^+$ TMSC-NV-treated group and the UVB group at a concentration of 100 μg/ml. However, Elastin expression increased by 5%, and MMP-13 expression decreased by 20% in the CD146$^+$ TMSC-NV-treated group compared with the UVB group (Figure 5b).

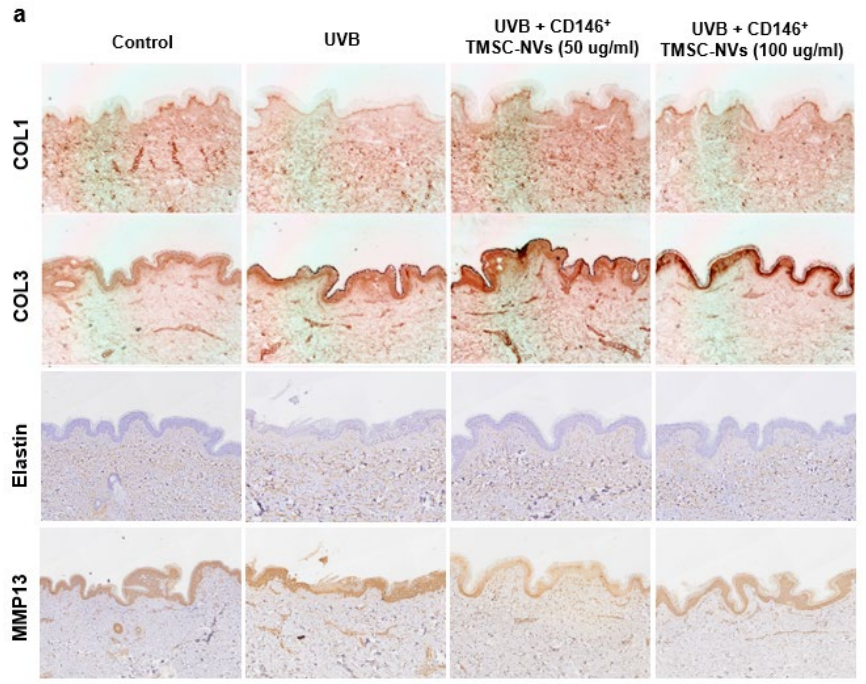

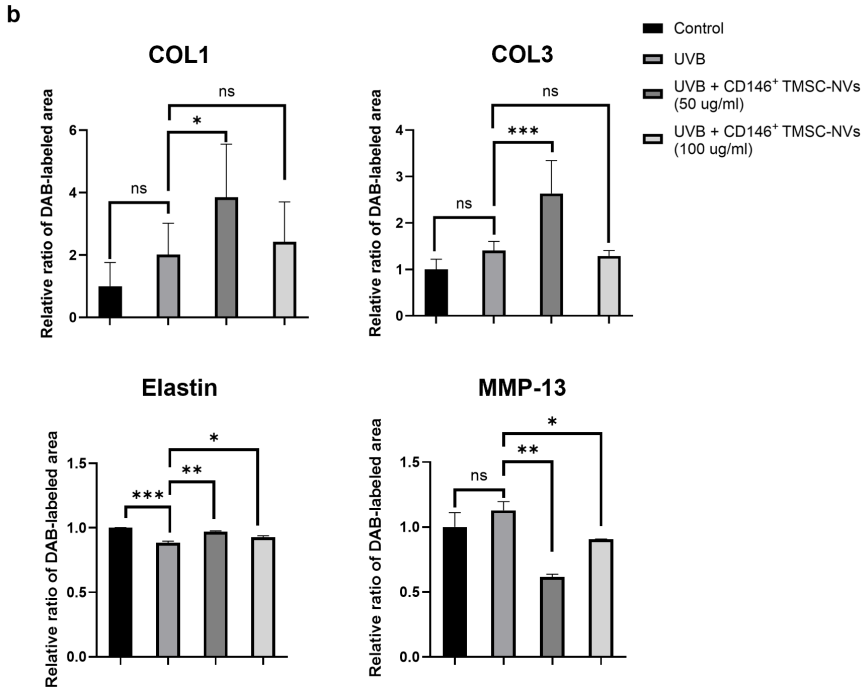

Figure 5. Regulation of Collagen type 1 (COL1), collagen type III (COL3), Elastin, and matrix metalloproteinase-13 (MMP-13) expression in the dermis by $CD146^+$ TMSC-NV treatment in an *ex vivo* model of human skin photoaging induced by ultraviolet B (UVB) radiation. (a) Immunohistochemical (IHC) analyses with DAB staining revealing that treatment with $CD146^+$ TMSC-NV at 50 μg/ml increased the staining for COL1, COL3, and Elastin compared with the UVB group while reducing MMP13 staining. (b) Quantitative analysis indicates a significant increase in the expression of COL1, COL3, and Elastin by 91%, 87%, and 10%, respectively, in the group treated with $CD146^+$ TMSC-NV of 50 μg/ml, compared with the UVB group. In contrast, MMP-13 expressions decreased by 45% relative to the UVB group. No significant differences in COL1 and COL3 levels were observed between the $CD146^+$ TMSC-NV-treated group and the UVB-treated group at a concentration of 100 μg/ml. However, Elastin expression increased by 5%, whereas MMP-13 expression decreased by 20% in the $CD146^+$ TMSC-NV-treated group compared with the UVB group ($p < 0.05$, ** $p < 0.01$, *** $p < 0.001$, **** $p < 0.0001$)

3.6. An *ex vivo* study of human skin photoaging models revealed that $CD146^+$ TMSC-NVs increased the expression of involucrin, filaggrin, and loricrin in the epidermis.

IHC analyses with DAB staining were conducted to assess the expression of involucrin, filaggrin, and loricrin proteins in the epidermis. Visual inspection revealed a decreased intensity of IHC DAB staining for involucrin, filaggrin, and loricrin in the epidermal layer of the UVB group compared to the control group. In contrast, treatment with $CD146^+$ TMSC-NV at 50 μg/ml increased the staining for involucrin, filaggrin, and loricrin compared with the UVB group (Figure 6a). These results were utilized for quantitative analysis to calculate the percentage of DAB-stained tissue, with DAB-stained regions marked on the original images. The results indicated a significant increase in the expression of involucrin, filaggrin, and loricrin by 250%, 340%, and 114%, respectively, in the group treated with $CD146^+$ TMSC-NV of 50 μg/ml compared with the UVB group. However, no significant differences were found in the levels of filaggrin and loricrin at a concentration of 100 μg/ml, except for involucrin expression, which demonstrated a 220% increase (Figure 6b).

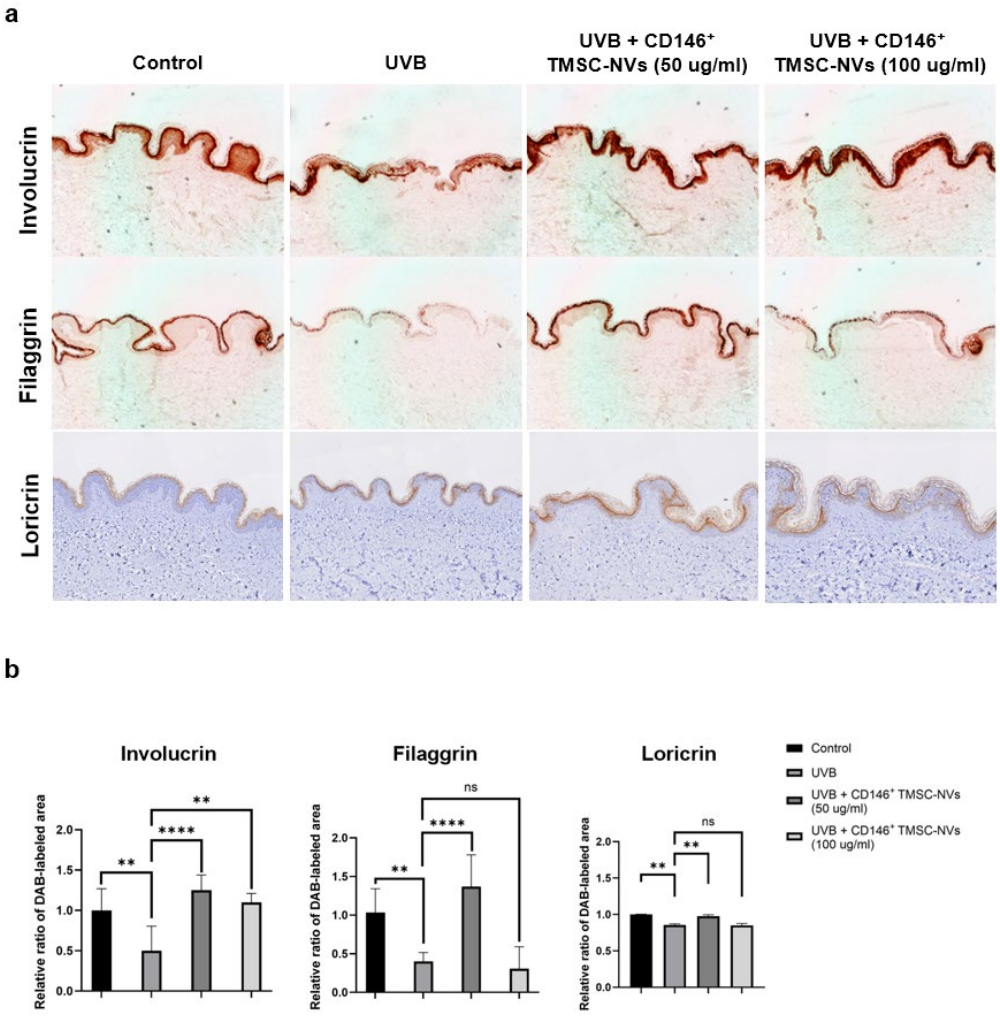

Figure 6. Regulation of Involucrin, Filaggrin, and Loricrin expression by treatment with $CD146^+$ TMSC-NVs in an ex vivo model of human skin photoaging induced by ultraviolet B (UVB) radiation (a) Immunohistochemical (IHC) analyses with DAB staining revealing that treatment with $CD146^+$ TMSC-NV at 50 μg/ml increased the staining for involucrin, filaggrin, and loricrin compared with the UVB group. (b) Quantitative analysis revealing a significant increase in involucrin, filaggrin, and loricrin expression by 250%, 340%, and 114%, respectively, in the group treated with $CD146^+$ TMSC-NV at 50 μg/ml compared with the UVB group. However, no significant differences were found in the levels of filaggrin and loricrin at a concentration of 100 μg/ml, except for involucrin expression, which demonstrated a 220% increase. (* $p < 0.05$, ** $p < 0.01$, *** $p < 0.001$, **** $p < 0.0001$)

3.7. An *in vivo* study of a natural aging mouse model revealed that CD146^{+} TMSC-NVs increased COL1 expression and decreased Elastin expression in the skin

Animal experiments were subsequently conducted based on the design summarized in Figure 7 following the antiaging properties of CD146^{+} TMSC-NVs demonstrated in old skin through *in vitro* and *ex vivo* studies. Briefly, CD146$^{+/-}$ TMSC-NVs were administered twice in the treatment group, with a 7-day interval between each administration. The control group was injected with PBS using the same procedure. The mice from all groups were sacrificed after completing the treatment regimen, and their skins were collected for histological analysis. Brain and liver tissues were harvested in addition to the skin to assess the potential antiaging effects on other organs. A comprehensive comparison of expression levels was conducted, including a comparison with the young group.

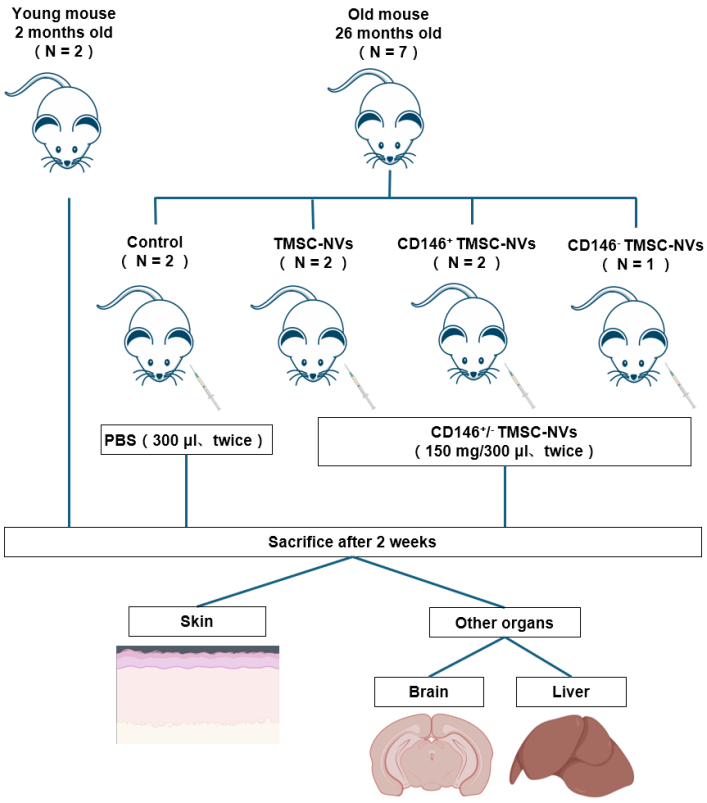

Figure 7. Experimental animals and CD146$^{+/-}$ TMSC-NV treatment. Intraperitoneal TMSC-NVs

were administered in four groups of old mice based on the injection material: Control (n = 2), TMSC-NVs (n = 2), CD146^{+} TMSC-NVs (n = 2), and CD146^{-} TMSC-NVs (n = 1). The treatment groups received two injections of TMSC-NVs at 150 μg/300 μl, with a 7-day interval between injections. In contrast, the control group received PBS of 300 μl. Young mice (n = 2) were included for interage comparisons from other groups. All mice were sacrificed after 2 weeks of administration, and their skin, brain, and liver were collected for further analysis.

H&E and MT staining in the skin revealed that the epidermal layer in the old mice was thinner with fewer cells. Additional qualitative changes, such as crypt formation from cell layer collapse and epidermal flattening, were observed. Collagen fibrils in the old skin appeared fragmented and irregularly distributed at the dermal level compared to the young skin. In contrast, old skin treated with CD146^{+} TMSC-NVs demonstrated more densely packed and well-organized collagen fibrils, whereas CD146^{-} TMSC-NV treatment did not cause any notable structural changes (Figure 8a).

IHC staining was utilized to evaluate COL1 and Elastin expression. Visual inspection revealed a decreased intensity of IHC DAB staining for COL1 in the old skin compared to the young skin, whereas Elastin demonstrated an increased density. In contrast, CD146^{+} TMSC-NV treatment increased the staining for COL1 and decreased the staining for Elastin, compared with the old skin. These results were utilized for quantitative analysis to calculate the percentage of stained tissue, with the stained regions marked on the original images. The relative expression of COL1 decreased by 8% in the old skin compared to the young skin, whereas Elastin expression increased by 10%. TMSC-NV, CD146^{+} TMSC-NV, and CD146^{-} TMSC-NV treatment significantly increased the COL1 expression in the old skin by 11%, 14%, and 7%, respectively, compared with the untreated old skin. However, only the CD146^{+} TMSC-NVs treatment demonstrated a 5% decrease in Elastin expression (Figure 8b). These results indicate that CD146^{+} TMSC-NVs may play a therapeutic role in antiaging effects on the skin.

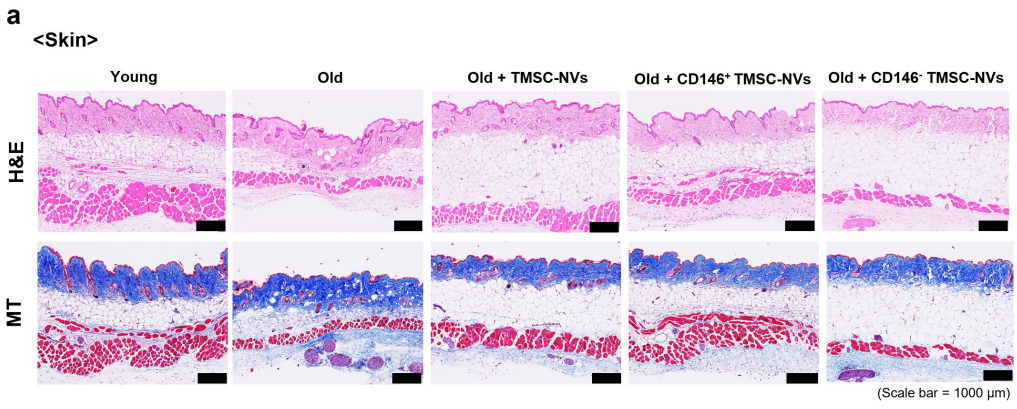

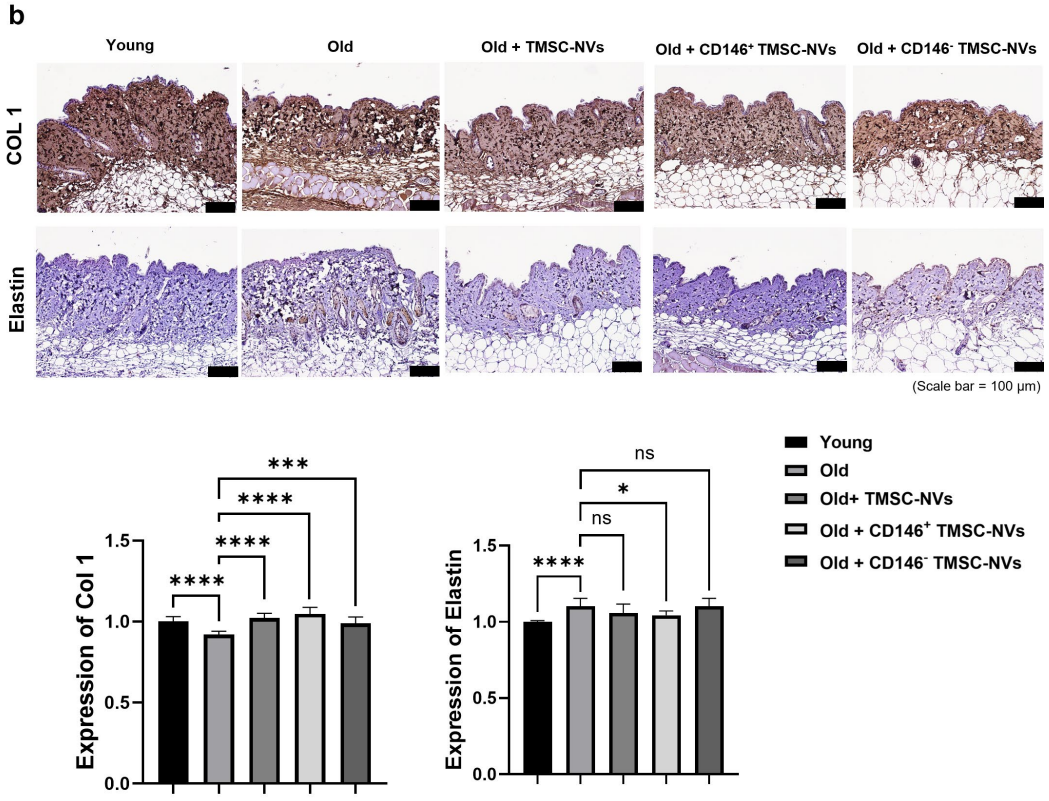

Figure 8. Histological analysis of skin in an *in vivo* study of a natural aging mouse model. (a) H&E and Masson's Trichrome (MT) staining revealed that the old skin treated with $CD146^+$ TMSC-NVs demonstrated a higher density and well-organized collagen fibrils, in comparison to the old control skin, exhibiting fragmented and irregularly distributed collagen fibrils. (b) Immunohistochemical staining was conducted to assess COL1 and Elastin expression. The relative COL1 expression by 8% was decreased in old skin compared to young skin, whereas Elastin expression was increased by 10%. In contrast, TMSC-NV, $CD146^+$ TMSC-NV, and $CD146^-$ TMSC-NV treatment significantly increased the COL1 expression in the old skin by 11%, 14%, and 7%, respectively, compared with the untreated old skin. However, only the $CD146^+$ TMSC-NV treatment demonstrated a 5% decrease in Elastin expression. These results indicate that $CD146^+$ TMSC-NVs upregulate the relative expression of COL1 and downregulate the expression of Elastin. (* $p < 0.05$, ** $p < 0.01$, *** $p < 0.001$, **** $p < 0.0001$)

3.8. Histological analysis of the brain and liver in an *in vivo* study of a

natural aging mouse model.

3.8.1 CD146$^+$ TMSC-NVs decreased the expression of p-Tau and Aβ in brain.

We harvested brain tissue in addition to the skin to assess the antiaging properties of CD146$^+$ TMSC-NVs. IHC staining was conducted to assess the expression of phospho-tau (p-Tau) and amyloid beta (Aβ). The relative expression of p-Tau was significantly increased in the old mice, demonstrating a 215% increase compared with the young mice. However, the CD146$^+$ TMSC-NVs treatment group exhibited a significant reduction in p-Tau expression by 47% compared with the old group, resembling the levels observed in the young group. The differences were not statistically significant, but Aβ expression in the old group was increased by 145% compared with that in the young group. In contrast, the CD146$^+$ TMSC-NVs treatment group demonstrated a significant reduction in Aβ expression by 41% compared with the old group (Figure 9a).

Moreover, we conducted Western blot analysis to investigate the expression of p-Tau and Aβ in the brain. The results were consistent with the IHC results, demonstrating increased p-Tau and Aβ expression in the old group compared with the young group. The CD146$^+$ TMSC-NVs treatment group demonstrated lower p-Tau and Aβ expression levels compared with the old group, whereas CD146$^-$ TMSC-NVs exhibited higher expression levels. Among all the treatment groups, the TMSC-NVs group showed the lowest p-Tau and Aβ expression levels (Figure 9b). These results indicate that CD146$^+$ TMSC-NVs may play a therapeutic role in antiaging effects on the brain.

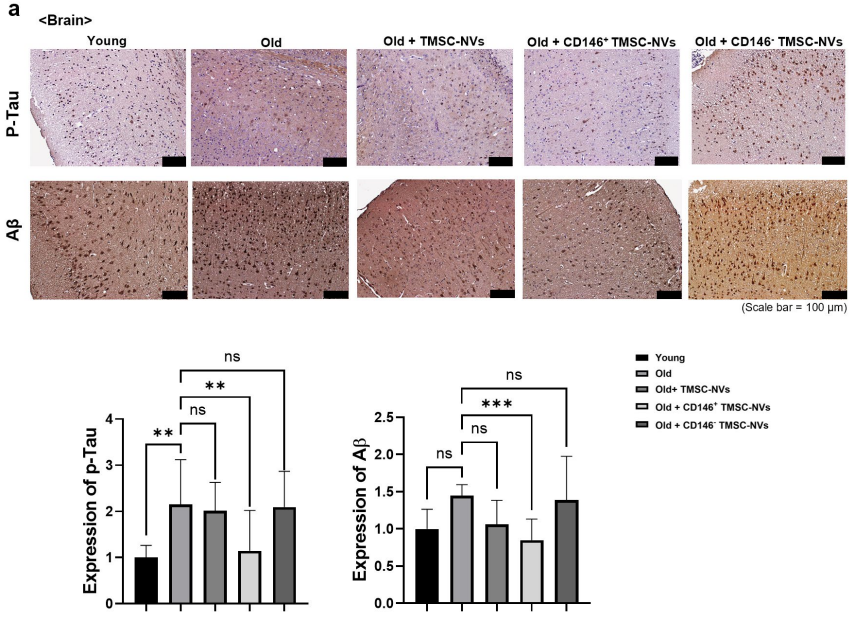

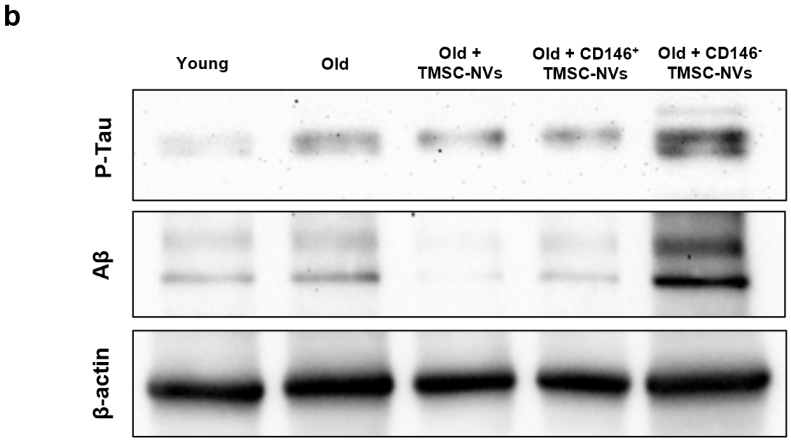

Figure 9. Histological analysis of the brain in an *in vivo* study of a natural aging mouse model. (a) Immunohistochemical staining was conducted to assess the expression of phospho-tau (p-Tau) and amyloid beta (Aβ), which are two critical factors in the pathophysiology of Alzheimer's disease (AD). The relative expression of p-Tau and Aβ in the old brain was increased by 215% and 145% compared with the young brain. However, the $CD146^+$ TMSC-NVs treatment group exhibited a significant reduction in p-Tau and Aβ expression by 47% and 41% compared to the old group, resembling the levels observed in the young group. (b) Western blot analysis revealed that the p-Tau and Aβ expression increased in the old brain compared to the young brain. The $CD146^+$ TMSC-NVs treatment group demonstrated lower p-Tau and Aβ expression levels compared with the old group, whereas $CD146^-$ TMSC-NVs demonstrated higher expression levels. (* $p < 0.05$, ** $p < 0.01$, *** $p < 0.001$, **** $p < 0.0001$)

3.8.2 $CD146^+$ TMSC-NVs decreased the expression of α-SMA in Liver

The expressions of α-SMA, a marker of liver fibrosis, and Perilipin-1, a marker of hepatic steatosis, were assessed in the liver using IHC staining. The relative expression of α-SMA was significantly increased in the old group, demonstrating a 125% increase compared with the young group. All treatment groups, including TMSC-NVs, $CD146^+$ TMSC-NVs, and $CD146^-$ TMSC-NVs, demonstrated reductions in α-SMA expressions by 16%, 24%, and 38%, respectively, compared with the old group. No statistically significant differences were observed between the young and old groups, but perilipin-1 was higher in the old group than in the young group. However, no significant differences were found in perilipin-1 expression among the old and all treatment groups (Figure 10).

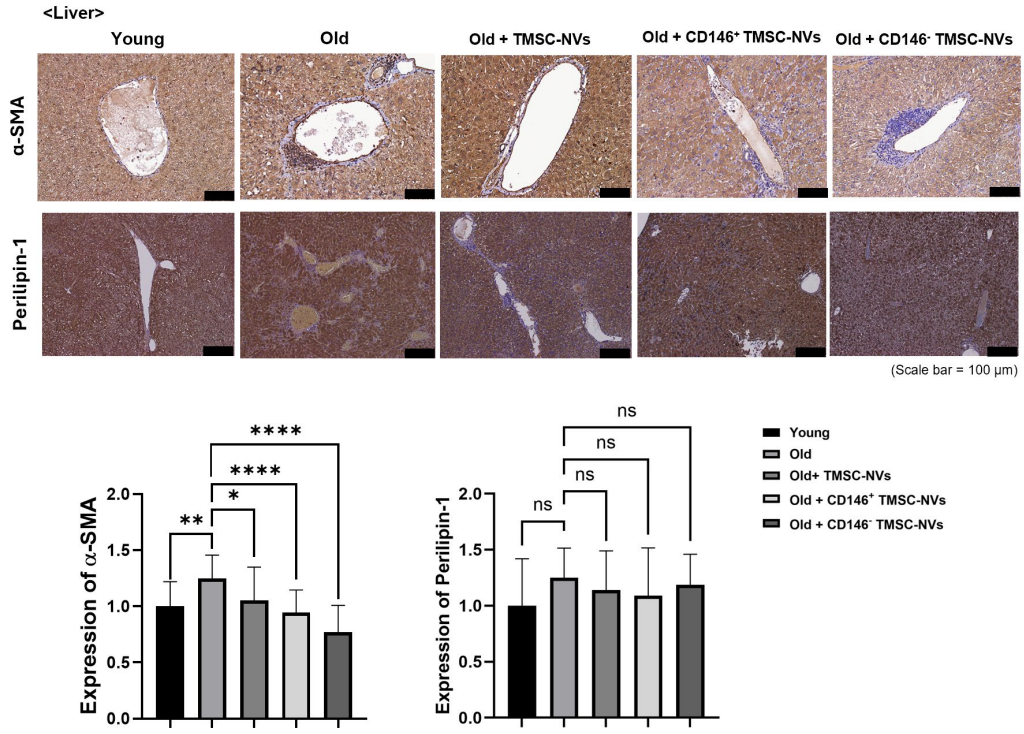

Figure 10. Histological analysis of the skin in an *in vivo* study of a natural aging mouse model. Immunohistochemical staining was conducted to evaluate alpha-smooth muscle actin (α-SMA) expression for liver fibrosis and perilipin-1 for hepatic steatosis. The relative expression of α-SMA increased by 125% in the old group compared with the young group. All treatment groups, including TMSC-NVs, $CD146^+$ TMSC-NVs, and $CD146^-$ TMSC-NVs α-SMA, exhibited reductions in α-SMA expressions by 16%, 24%, and 38%, respectively, compared with the old group. Furthermore, no statistically significant differences were observed between the young and old groups, but perilipin-1 was higher in the old group than in the young group. However, no significant differences were found in perilipin-1 expression among the old and all treatment groups. (* $p < 0.05$, ** $p < 0.01$, *** $p < 0.001$, **** $p < 0.0001$)

IV. Discussion.

This study investigated the potential antiaging properties of $CD146^+$ TMSC-NVs through *in vitro*, *ex vivo*, and *in vivo* models. A previous study revealed that TMSC-NVs improved cell proliferation and reduced senescence in old HDF.[10] The results indicate that TMSC-NVs served as an alternative to exosomes for skin rejuvenation, but the mechanisms by which TMSC-NVs

regulate cellular senescence remain unclear. Therefore, in a future study, we plan to determine the key markers of TMSC-NVs involved in cellular senescence regulation

CD146, a member of the immunoglobulin superfamily, was originally determined for its role in promoting melanoma growth and metastasis.[20] However, recent studies have demonstrated its potential as a surface marker for determining specific subgroups of MSCs. CD146 is now recognized as an early mesenchymal marker in MSCs derived from different sources, including the bone marrow, dental pulp, adipose tissue, and umbilical cord.[11] This study further highlighted the crucial role of CD146 in stem cell biology, particularly its relevance to aging and regenerative therapies.

Old MSCs typically demonstrate a reduction in CD146 expression, which is correlated with decreased proliferative and differentiation capabilities. This indicates that CD146 is a useful marker for evaluating the quality and senescence status of MSCs, which is crucial for ensuring the efficacy of MSC-based therapies.[21] Several studies have revealed that $CD146^+$ MSCs demonstrate superior multilineage differentiation potential and stronger immunomodulatory effects *in vitro* compared to $CD146^-$ cells.[22] Furthermore, CD146 expression has been closely related to increased proliferation and angiogenesis in adipocyte-derived MSCs, indicating its broader role in promoting tissue repair and regeneration.[23] These results, particularly in the context of aging and the development of antiaging therapies, emphasize the need for further investigation into the molecular mechanisms by which CD146 affects cellular senescence and regeneration.

This study categorized the cells into CD146-positive ($CD146^+$) and CD146-negative ($CD146^-$) cells using MACS after confirming the characteristic identification of TMSCs. NVs derived from TMSCs (TMSC-NVs), $CD146^+$ TMSCs ($CD146^+$ TMSC-NVs), and $CD146^-$ TMSCs ($CD146^-$ TMSC-NVs) were manufactured. These significantly improved cell proliferation and reduced senescence-associated β-galactosidase activity in old HDFs *in vitro*, whereas $CD146^-$ TMSC-NVs did not exhibit a similar effect. The qPCR analysis revealed that the mRNA expression of ECM and antioxidant genes related to cellular senescence was upregulated in old HDFs treated with $CD146^+$ TMSC-NVs compared with those treated with $CD146^-$ TMSC-NVs. These results indicate that $CD146^+$ TMSC-NVs decreased cellular senescence and increased cell proliferation, antioxidant gene expression, and ECM production, unlike $CD146^-$ TMSC-NVs. Microarray analysis was conducted to further assess the effect of $CD146^+$ TMSC-NVs on the gene expression profile of HDFs. The results indicated that senescence-related genes were differentially expressed in HDFs treated with $CD146^+$ TMSC-NVs compared with old HDFs, with the gene expression profile closely resembling that of young HDFs. Furthermore, the KEGG pathway demonstrated that $CD146^+$ TMSC-NVs downregulate the cellular senescence pathway at the gene level. Therefore, we indicate that $CD146^+$ TMSC-NVs reduce cellular senescence and demonstrate antiaging effects on the skin in an *in vitro* study.

Based on these results, $CD146^+$ TMSC-NVs were applied to an *ex vivo* model of human skin photoaging induced by UVB radiation. IHC analyses with DAB staining were conducted to assess the expression of epidermis marker proteins (involucrin, filaggrin, and loricrin) and dermis marker proteins (COL1, COL3, Elastin, and MMP-13). Human skin aging is categorized into two distinct processes: intrinsic aging, which occurs as a natural consequence of time, and extrinsic aging,

which is primarily driven by environmental factors, with UV exposure being a major contributor. Prolonged UV exposure accelerates the aging process, causing epidermal thinning and collagen and elastic fiber breakdown within the dermis. This degradation is accompanied by dysfunctional Elastin accumulation, a hallmark of solar elastosis, which contributes to the skin's reduced elasticity and structural integrity.[24] Additionally, UV stimulates reactive oxygen species production, which subsequently upregulates the expression of metalloproteases (MMPs). These enzymes play a crucial role in degrading the ECM, thereby further contributing to skin aging and structural decline.[25]

COL1, COL3, and Elastin are fundamental to maintaining the skin's structural integrity, elasticity, and tensile strength in the dermis layer, thereby forming the ECM. These proteins are highly vulnerable to degradation by UV radiation, which accelerates skin aging and weakens the ECM.[26] MMP-13, also known as collagenase-3, is especially active in degrading collagen under UV exposure, contributing significantly to collagen fiber breakdown and subsequent skin deterioration.[27] A significant increase in the expression of COL1, COL3, and Elastin accompanied by a reduction in MMP-13 expression was observed in the group treated with $CD146^+$ TMSC-NVs of 50 μg/ml compared with the UVB group.

Essential proteins, such as filaggrin, involucrin, and loricrin, play a crucial role in maintaining the skin barrier function, especially in response to UV radiation, in the epidermal layer.[28] Filaggrin is vital for skin hydration and overall barrier integrity, whereas involucrin contributes to the skin's mechanical stability in the upper epidermal layers.[29] Loricrin is a major constituent of the cornified envelope, providing elasticity and strength to the skin barrier.[30] UV radiation exposure disrupts the expression of these proteins, thereby compromising the protective barrier and making the skin more susceptible to dehydration, damage, and photoaging.[31] The results revealed that treatment with $CD146^+$ TMSC-NVs at 50 μg/ml caused a significant increase in involucrin, filaggrin, and loricrin expression in UVB-exposed models. Therefore, we indicate that $CD146^+$ TMSC-NVs promote ECM and epidermis regeneration, emphasizing their potential for skin rejuvenation applications in an *ex vivo* skin model.

Subsequent animal experiments were conducted to evaluate the antiaging effects of $CD146^+$ TMSC-NVs in an *in vivo* study of a natural aging mouse model. In this study, IP TMSC-NVs were administered in a natural aging mouse model. IP administration, which involves delivering a drug directly into the peritoneal cavity, is a practical and widely used method for *in vivo* studies in rodents. Intravenous (IV) administration generally achieves higher drug bioavailability, but it is often less practical for rodent studies due to technical complexity, particularly in smaller animals, such as mice, and its limitations for repeated dosing. In contrast, the IP administration technique provides several advantages, including procedural safety, reliable therapeutic bioavailability for both small and large molecules, versatility in application, suitability for long-term treatments, and ease of execution.[32] Additionally, it enables the drug to circulate, interact with immune cells, and potentially integrate into different tissues throughout the body. In particular, IP administration for small-molecule pharmacological agents caused accelerated and more complete absorption compared to oral and subcutaneous routes.[33] Therefore, we performed IP TMSC-NVs administration in four groups of old mice, each receiving different treatments: control (n = 2),

TMSC-NVs (n = 2), CD146$^+$ TMSC-NVs (n = 2), and CD146$^-$ TMSC-NVs (n = 1). The treatment groups received two doses of TMSC-NVs at 150 μg/300 μl, administered at a 7-day interval, whereas the control group was given PBS of 300 μl. Additionally, young mice (n = 2) were included to enable inter-age comparisons. All mice were sacrificed two weeks after the second injection, and their skin, brain, and liver were collected for further analysis

The epidermis thins and the dermo-epidermal junction flattens in aging skin. The dermis becomes atrophic, characterized by a reduced number and size of collagen fiber bundles, the loss of the elastic network perpendicular to the epidermis, and the deterioration of the deeper elastic network.[34] In this study, CD146$^+$ TMSC-NVs-treated skin demonstrated improved collagen fibril density and organization compared with the old skin, exhibiting fragmented and irregular collagen distribution. Notably, the relative expression of COL1 in the dermis of old skin was reduced compared with that of young skin, whereas Elastin levels were elevated. This is consistent with previous studies that have revealed a decreased collagen content and an increased elastic fiber abundance in aging mouse skin.[34] The observed increase in the elastic fibers in aging skin may represent a compensatory mechanism to provide structural support as the superficial layers are thin. In contrast, CD146$^+$ TMSC-NVs treatment upregulated the relative expression of COL1 and downregulated the Elastin expression in the skin. These results indicate that CD146$^+$ TMSC-NVs may play a therapeutic role in the antiaging effects on the skin..

We planned to assess the effects of CD146$^+$ TMSC-NVs following IP administration on other organs in addition to the skin. IP administration is expected to predominantly affect the abdominal organs, including the liver, spleen, and intestines, rather than a more distant brain with its inherent brain-blood barrier (BBB).[35] The BBB is a highly selective semipermeable barrier that protects the brain from potentially harmful substances in the bloodstream, including most cells, drugs, and larger molecules. However, NVs exhibit a significant advantage over stem cells in terms of crossing the BBB, due to their small size and capacity to be internalized by brain endothelial cells.[36] Some studies revealed that brain exposure to small molecular drugs was greater after IP compared to IV infusion regarding the route of administration. This may be attributed to the saturation of transporters at the BBB and accelerated clearance after IV infusion.[37] Therefore, we investigated the effect of the TMSC-NVs after IP administration on the aging brain. The relative expression of p-Tau and Aβ was higher in the brain in the old mice than in the young mice. Amyloid-β and Tau proteins have been widely recognized as key contributors to the pathophysiology of AD, largely due to their accumulation in hallmark histopathological lesions and increased levels of their soluble forms in the brains of patients with AD.[38] In this study, IHC analysis and western blot revealed a significant reduction in the expression of p-Tau and Aβ in the CD146$^+$ TMSC-NVs-treated group compared with the old group. These results indicate that CD146$^+$ TMSC-NVs may play a role in downregulating p-Tau and Aβ expression, demonstrating potential neuroprotective effects. Further investigation is warranted to determine the mechanisms by which CD146$^+$ TMSC-NVs affect the p-Tau and Aβ pathways and their potential therapeutic applications for neurodegenerative diseases such as AD.

The liver tissue was harvested for histological analysis to assess the direct effects of IP administration using TMSC-NVs. The expression of α-SMA and perilipin-1 in the liver was

assessed using IHC staining. α-SMA is widely recognized as a reliable biomarker for assessing liver fibrosis, as its levels strongly correlate with fibrosis severity.[39] Similarly, perilipin-1, predominantly expressed by mature adipocytes, is mainly observed in large lipid droplets and plays a role in developing macrovesicular steatosis in hepatocytes.[40] In this study, significant differences in the expression of α-SMA were found between the old and young groups. The $CD146^+$ TMSC-NVs treatment group demonstrated a significant decrease compared with the old group. These results indicate that TMSC-NVs exerted antifibrotic effects on liver fibrosis. However, no significant differences were observed in the expression of perilipin-1 between each group. Further investigation is warranted to identify whether alternative dosing strategies or treatment durations yield different outcomes, particularly for potential therapeutic applications of TMSC-NVs in fatty liver disease.

This study demonstrated significant results, but several limitations must be recognized, and further investigation is warranted. The small sample size in the natural aging mouse model may reduce the generalizability, precision, and reliability of the results. Additionally, natural aging models present challenges due to their time-consuming, labor-intensive, and costly nature. Similarly, most old mice died over time in this study, thereby significantly reducing the number of mice in the sample. Hence, researchers often prefer induced accelerated aging models because they provide readily available resources, shorter modeling times, and consistent aging effects.[41] Future studies are warranted to validate and refine these results, potentially by increasing the sample size within the induced accelerated aging model. Another limitation is the absence of a defined therapeutic range, making it difficult to accurately identify the optimal dose of $CD146^+$ TMSC-NVs for injection. The route, dose, and frequency of NVs administration in this study were based on a previous study.[14] However, other studies have utilized different methods for dose and frequency when assessing antiaging effects in aging mouse models.[42] Standardization of these parameters is crucial to ensure both effectiveness and consistency before proceeding to clinical applications. Therefore, further studies are warranted to establish standardized protocols for NVs administration. Overall, these limitations provide valuable information for future research to improve the understanding and application of $CD146^+$ TMSC-NVs in antiaging therapies.

V. Conclusions.

This study revealed that $CD146^+$ TMSC-NVs decreased cellular senescence and increased cell proliferation, ECM production, and antioxidant gene expression. Microarray analysis revealed that senescence-related genes were differentially expressed in $CD146^+$ TMSC-NVs-treated HDFs compared with untreated old HDFs, indicating a cellular senescence pathway downregulation at the gene level. Subsequently, an *ex vivo* model of human skin photoaging induced by UVB radiation revealed that $CD146^+$ TMSC-NVs increased ECM and epidermal production, emphasizing their potential for applications in skin rejuvenation. The natural aging mouse model demonstrated that $CD146^+$TMSC-NVs increased COL1 expression and decreased Elastin

expression.

The brain and liver, in addition to the skin, were analyzed to assess the antiaging properties of $CD146^+$ TMSC-NVs. $CD146^+$ TMSC-NVs appeared to downregulate p-Tau and Aβ expression in the brain, indicating potential neuroprotective effects. Additionally, α-SMA expression in the liver was reduced in the TMSC-NVs-treated groups compared with the untreated old group, indicating potential antifibrotic effects. However, no significant differences in the perilipin-1 expression were observed between the old and TMSC-NVs-treated groups.

In conclusion, CD146+ TMSC-NVs effectively reduce cellular senescence and reverse aging in the skin, brain, and liver of mouse models. These results indicate the significant therapeutic potential of $CD146^+$ TMSC-NVs in antiaging treatments.

References

1. Zhou C, Elshkaki A, Graedel TE. Global Human Appropriation of Net Primary Production and Associated Resource Decoupling: 2010-2050. Environ Sci Technol 2018;52:1208-15.
2. Wisensale SK. Global Aging and Intergenerational Equity. Journal of Intergenerational Relationships 2003;1:29-47.
3. Liang J-X, Liao X, Li S-H, Jiang X, Li Z-H, Wu Y-D, et al. Antiaging Properties of Exosomes from Adipose-Derived Mesenchymal Stem Cells in Photoaged Rat Skin. BioMed Research International 2020;2020:6406395.
4. López-Otín C, Blasco MA, Partridge L, Serrano M, Kroemer G. The hallmarks of aging. Cell 2013;153:1194-217.
5. Dodig S, Čepelak I, Pavić I. Hallmarks of senescence and aging. Biochem Med (Zagreb) 2019;29:030501.
6. Son HY, Bae HS, Son Y, Kim S, Hong HS, Park JU. Biological Aging Parameters Can Be Improved After Autologous Adipose-Derived Stem Cell Injection. J Craniofac Surg 2019;30:652-8.
7. Borghesan M, Fafián-Labora J, Eleftheriadou O, Carpintero-Fernández P, Paez-Ribes M, Vizcay-Barrena G, et al. Small Extracellular Vesicles Are Key Regulators of Non-cell Autonomous Intercellular Communication in Senescence via the Interferon Protein IFITM3. Cell Reports 2019;27:3956-71.e6.
8. Kim Y-J, Yoo Sm, Park HH, Lim HJ, Kim Y-L, Lee S, et al. Exosomes derived from human umbilical cord blood mesenchymal stem cells stimulates rejuvenation of human skin. Biochemical and Biophysical Research Communications 2017;493:1102-8.
9. Li X, Corbett AL, Taatizadeh E, Tasnim N, Little JP, Garnis C, et al. Challenges and opportunities in exosome research—Perspectives from biology, engineering, and cancer therapy. APL Bioengineering 2019;3.
10. Kim D, Lee Y, Park K, Park D, Lee WJ, Roh TS, et al. Anti-Aging Effects of Nanovesicles Derived from Human Tonsil-Derived Mesenchymal Stem Cells. Applied Sciences 2021;11.
11. Wu C-C, Liu F-L, Sytwu H-K, Tsai C-Y, Chang D-M. CD146+ mesenchymal stem cells display greater therapeutic potential than CD146– cells for treating collagen-induced arthritis in mice. Stem Cell Research & Therapy 2016;7:23.
12. Zhang L, Sun Y, Zhang X-X, Liu Y-B, Sun H-Y, Wu C-T, et al. Comparison of CD146 +/− mesenchymal stem cells in improving premature ovarian failure. Stem Cell Research & Therapy 2022;13:267.
13. Zhang L, Zhang X, Liu Y, Zhang W, Wu CT, Wang L. CD146+ Umbilical Cord Mesenchymal Stem Cells Exhibit High Immunomodulatory Activity and Therapeutic Efficacy in Septic Mice. J Inflamm Res 2023;16:579-94.
14. Li Z, Liu Y, Tian Y, Li Q, Shi W, Zhang J, et al. Human umbilical cord mesenchymal stem cell-derived exosomes improve ovarian function in natural aging by inhibiting apoptosis. Int J Mol Med 2023;52.

15. Kanehisa M, Goto S. KEGG: kyoto encyclopedia of genes and genomes. Nucleic Acids Res 2000;28:27-30.
16. Dennis G, Jr., Sherman BT, Hosack DA, Yang J, Gao W, Lane HC, et al. DAVID: Database for Annotation, Visualization, and Integrated Discovery. Genome Biol 2003;4:P3.
17. Huang da W, Sherman BT, Lempicki RA. Systematic and integrative analysis of large gene lists using DAVID bioinformatics resources. Nat Protoc 2009;4:44-57.
18. Schindelin J, Arganda-Carreras I, Frise E, Kaynig V, Longair M, Pietzsch T, et al. Fiji: an open-source platform for biological-image analysis. Nature Methods 2012;9:676-82.
19. Thacker JS, Andersen D, Liang S, Zieniewicz N, Trivino-Paredes JS, Nahirney PC, et al. Unlocking the brain: A new method for Western blot protein detection from fixed brain tissue. J Neurosci Methods 2021;348:108995.
20. Lehmann JM, Riethmüller G, Johnson JP. MUC18, a marker of tumor progression in human melanoma, shows sequence similarity to the neural cell adhesion molecules of the immunoglobulin superfamily. Proceedings of the National Academy of Sciences 1989;86:9891-5.
21. Jin HJ, Kwon JH, Kim M, Bae YK, Choi SJ, Oh W, et al. Downregulation of Melanoma Cell Adhesion Molecule (MCAM/CD146) Accelerates Cellular Senescence in Human Umbilical Cord Blood-Derived Mesenchymal Stem Cells. Stem Cells Transl Med 2016;5:427-39.
22. Tsang WP, Shu Y, Kwok PL, Zhang F, Lee KK, Tang MK, et al. CD146+ human umbilical cord perivascular cells maintain stemness under hypoxia and as a cell source for skeletal regeneration. PLoS One 2013;8:e76153.
23. Lauvrud AT, Kelk P, Wiberg M, Kingham PJ. Characterization of human adipose tissue-derived stem cells with enhanced angiogenic and adipogenic properties. J Tissue Eng Regen Med 2017;11:2490-502.
24. Lynch B, Pageon H, Le Blay H, Brizion S, Bastien P, Bornschlögl T, et al. A mechanistic view on the aging human skin through ex vivo layer-by-layer analysis of mechanics and microstructure of facial and mammary dermis. Scientific Reports 2022;12:849.
25. Pillai S, Oresajo C, Hayward J. Ultraviolet radiation and skin aging: roles of reactive oxygen species, inflammation and protease activation, and strategies for prevention of inflammation-induced matrix degradation - a review. Int J Cosmet Sci 2005;27:17-34.
26. Zorina A, Zorin V, Kudlay D, Kopnin P. Molecular Mechanisms of Changes in Homeostasis of the Dermal Extracellular Matrix: Both Involutional and Mediated by Ultraviolet Radiation. International Journal of Molecular Sciences 2022;23:6655.
27. Xue N, Liu Y, Jin J, Ji M, Chen X. Chlorogenic Acid Prevents UVA-Induced Skin Photoaging through Regulating Collagen Metabolism and Apoptosis in Human Dermal Fibroblasts. International Journal of Molecular Sciences 2022;23:6941.
28. Furue M. Regulation of Filaggrin, Loricrin, and Involucrin by IL-4, IL-13, IL-17A, IL-22, AHR, and NRF2: Pathogenic Implications in Atopic Dermatitis. Int J Mol Sci 2020;21.
29. Armengot-Carbo M, Hernández-Martín Á, Torrelo A. The Role of Filaggrin in the Skin Barrier and Disease Development. Actas Dermo-Sifiliográficas 2015;106:86-95.

30. Bickenbach JR, Greer JM, Bundman DS, Rothnagel JA, Roop DR. Loricrin expression is coordinated with other epidermal proteins and the appearance of lipid lamellar granules in development. J Invest Dermatol 1995;104:405-10.
31. Li L, Liu Y, Chang R, Ye T, Li Z, Huang R, et al. Dermal Injection of Recombinant Filaggrin-2 Ameliorates UVB-Induced Epidermal Barrier Dysfunction and Photoaging. Antioxidants 2024;13:1002.
32. Al Shoyaib A, Archie SR, Karamyan VT. Intraperitoneal Route of Drug Administration: Should it Be Used in Experimental Animal Studies? Pharm Res 2019;37:12.
33. Durk MR, Deshmukh G, Valle N, Ding X, Liederer BM, Liu X. Use of Subcutaneous and Intraperitoneal Administration Methods to Facilitate Cassette Dosing in Microdialysis Studies in Rats. Drug Metab Dispos 2018;46:964-9.
34. Bhattacharyya TK, Thomas JR. Histomorphologic Changes in Aging Skin. Archives of Facial Plastic Surgery 2004;6:21-5.
35. Oberoi RK, Parrish KE, Sio TT, Mittapalli RK, Elmquist WF, Sarkaria JN. Strategies to improve delivery of anticancer drugs across the blood-brain barrier to treat glioblastoma. Neuro Oncol 2016;18:27-36.
36. Nouri Z, Barfar A, Perseh S, Motasadizadeh H, Maghsoudian S, Fatahi Y, et al. Exosomes as therapeutic and drug delivery vehicle for neurodegenerative diseases. Journal of Nanobiotechnology 2024;22:463.
37. Liu X, Van Natta K, Yeo H, Vilenski O, Weller PE, Worboys PD, et al. Unbound drug concentration in brain homogenate and cerebral spinal fluid at steady state as a surrogate for unbound concentration in brain interstitial fluid. Drug Metab Dispos 2009;37:787-93.
38. Gulisano W, Maugeri D, Baltrons MA, Fà M, Amato A, Palmeri A, et al. Role of Amyloid-β and Tau Proteins in Alzheimer's Disease: Confuting the Amyloid Cascade. J Alzheimers Dis 2018;64:S611-s31.
39. Akpolat N, Yahsi S, Godekmerdan A, Yalniz M, Demirbag K. The value of alpha-SMA in the evaluation of hepatic fibrosis severity in hepatitis B infection and cirrhosis development: a histopathological and immunohistochemical study. Histopathology 2005;47:276-80.
40. Sharma A. Lipid droplets associated perilipins protein insights into finding a therapeutic target approach to cure non-alcoholic fatty liver disease (NAFLD). Future Journal of Pharmaceutical Sciences 2022;8:1.

Abstract in Korean

인간 편도 유래 중간엽 줄기세포에서 추출한 CD146+ 나노 소포체의 항노화 효과

출산율의 감소와 기대수명의 증가로 인해 전 세계 고령화는 전례 없는 수준에 이를 것으로 예상된다. 이러한 변화는 다양한 질병의 발병과 연관되어 사회, 의료 시스템 및 경제에 상당한 부담을 안겨주고 있다. 이에 항노화와 관련된 연구가 활발히 진행되고 있으며 줄기 세포 기반 치료법이 각광받고 있다. 하지만 줄기세포의 임상적 한계가 드러나면서 나노 크기의 생체 모방 소포체가 많은 관심을 받고 있다. 최근 연구에 따르면 편도 중간엽 줄기세포에서 추출한 나노 소포체는 세포 노화, 특히 산화 스트레스로 인한 노화를 역전시킬 수 있는 잠재력 있는 것으로 밝혀졌다. 이에 본 연구에서는 중간엽 줄기세포의 특정 하위 그룹을 식별하는 데 사용되는 표면 마커인 CD146에 집중하여 편도 유래 중간엽 줄기세포에서 추출한 $CD146^+$ 나노 소포체의 치료적 역할과 항노화 잠재력을 연구하였다. $CD146^+$ 나노 소포체를 인간 피부 섬유아세포의 노화 모델, 자외선 방사선에 의해 유도된 인간 피부 광노화의 생체 외 모델, 자연 노화 마우스 모델에 적용하였다. 연구 결과, $CD146^+$ 나노 소포체는 노화 섬유아세포에서 세포 증식을 촉진하고, 세포외기질 성분과 항산화 유전자의 유전자 발현을 향상시켰다. 또한 노화 관련 베타-락토시다제 활성을 감소시킨다는 사실을 밝혀 냈다. 항노화 효과의 기전을 유전자 수준에서 분석하기 위해 시행한 Microarray 분석 결과, $CD146^+$ 나노 소포체로 처리된 섬유아세포는 처리되지 않은 노화 섬유아세포와 비교하여 노화 관련 유전자의 발현이 차별적으로 나타났으며, 이는 젊은 HDF의 유전자 발현과 매우 유사하게 나타났다. 또한 $CD146^+$ 나노 소포체는 세포 노화 경로의 특정 유전자 발현을 억제하여 세포 노화를 막는다는 것을 확인할 수 있었다.

방사선에 의해 유도된 인간 피부 광노화의 생체 외 모델에서는 50 μg/ml의 $CD146^+$ 나노 소포체를 처리한 그룹에서 방사선 조사 그룹에 비해 Collagen과 Elastin의 발현이 유의미하게 증가하였고, MMP-13의 발현은 감소했다. 또한 표피에서도 피부 방어 기능이 있는 Involucrin, Filaggrin, Loricrin의 발현이 유의하게 증가하였다. 이러한 결과는 CD146+ 나노 소포체가 진피의 세포외기질과 표피 생성을 증가시켜 피부에서의 항노화 효과 가능성을 보여주었다.

또한 자연 노화 마우스 모델에서 $CD146^+$ 나노 소포체는 피부에서 collagen type 1의 발현을 증가시키고 Elastin의 발현은 감소시켰으며, 뇌에서는 노화된 쥐 그룹에 비해 phostphorylated Tau와 Amyloid-β의 발현을 감소시켰다. 간에서는 간섬유화를 확인할 수 있는 α-SMA의 상대적 발현이 치료하지 않은 늙은 피부에

비해 치료 그룹에서 유의미하게 감소했다. 그러나 prilipin-1 발현은 노화된 쥐와 치료 그룹 간에 유의미한 차이는 없었다.

결론적으로, 세포 실험에서 인간 편도 유래 줄기세포로부터 추출한 $CD146^+$ 나노소포체는 세포 노화를 효과적으로 감소시켰으며, 노화된 쥐의 피부, 뇌, 간 조직의 실험에서도 노화 방지 치료를 위한 치료 전략으로서 상당한 잠재력을 제공한다는 결과를 얻을 수 있었다.

핵심되는 말: 중간엽 줄기세포; 세포 유래 미세 입자; 세포 노화

Supplemental Figure S1. Kyoto Encyclopedia of Genes and Genomes (KEGG) pathway enrichment analyses of differentially expressed genes were performed, comparing the old group with other groups.